

Scuola di Ingegneria Industriale e dell'Informazione

Corso di Laurea Magistrale in Materials Engineering and Nanotechnology

Chemistry and Materials Engineering department Giulio Natta

Study and Modellization of Mechanoluminescent Materials



Thesis by Luca Seghizzi 837201

Supervisor

Professor David Bucknall Heriot Watt University Edinburgh

Examination Committee

Professor Fabio Ganazzoli Politecnico di Milano

Academic year 2015/2016

Copyright

Luca Seghizzi

I would like to thank professor Fabio Ganazzoli who gave me the possibility to go to Edinburgh and make this project and professor David Bucknall and his colleagues who helped me a lot, supported me and were always available for clarifications and explanations.

Lot of thanks are due to all the friends I have met in my life, in hometown and during my childhood, as well as my university companions and all the other people around the world that have made me smile and understand that a hand will always arrive even if distance is in between us.

Moreover, a huge thank you for my parents who have always sustained me in all my experiences, who gave me the possibility to travel and study abroad and thanks to their teaching and education that has made me become the person I am today. I owe them everything.

A final thank you to my girlfriend, with whom I have spent these last six months in Edinburgh while working at this thesis project, who gave me happiness, peace and support in all the situations.

Abstract

Mechanoluminescence (ML) is the emission of light from some materials when a mechanical stimulus is applied to them. The most studied phosphors are ZnS crystals doped with Cu or Mn because they exhibit the brightest luminescent emission. For practical applications, embedding them in a polymer matrix like PDMS is very promising because flexible and stretchable mechanoluminescent devices can be created.

However, the phenomenon is not yet fully understood, there are commercially available powders produced from big industries that exhibit the phenomena and basic devices build on using PDMS. There is the need to understand it more deeply, to develop the technology and develop its hidden potential to create more interesting applications using this phenomenon.

Since a lot of questions are unresolved and not present in literature, the aim of this thesis is to find the basic concepts and mechanism for a more complete study. During the development of the project, four main points will be studied.

- Mechanoluminescent introduction and detailed explanation of all the phenomena related to it
- Setting the experiment and detection of mechanoluminescence of some simple devices
- The finite element analysis is one of the most powerful tool to understand and solve engineering problems and therefore make a correct and precise model is needed for further studies and for a deeper understanding. Moreover, it turns out to be difficult to produce an accurate model for the analysis, especially concerning the sample geometry. Therefore, it was developed a way to create meshes from pictures using some simple codes in Matlab and Python.

- Finally, a new theory based on mechanoluminescence will be discussed and an experimental verification of the theory will be shown.

A more extensive analysis and experimental study have to be done to understand fully the phenomenon and improve it but this thesis will provide some basic concepts, analysis techniques and experimentation procedure to produce ML phosphors and devices.

Estratto in Italiano

La meccanoluminescenza è un fenomeno per cui un materiale emette luce quando è sottoposto ad uno sforzo meccanico. Vi sono diversi tipi di fosfori meccanoluminescenti disponibili sul mercato, ma il seguente studio si occuperà specialmente di capire il funzionamento di quelli più promettenti, le particelle di ZnS dopato con atomi di manganese o di rame.

Queste sono le più usate in quanto sono quelle che hanno il più basso valore di soglia dello stress per esibire il fenomeno della meccanoluminescenza e per cui sono più soggette a sperimentazioni per applicazioni pratiche.

Per capirne il funzionamento e riprodurle in laboratorio, diversi passaggi sono stati necessari e nei seguenti quattro capitoli verranno descritti in modo molto dettagliato.

È necessario innanzitutto un'ampia introduzione sul comportamento dei semiconduttori, sull'effetto piezoelettrico e sulla meccanoluminescenza per capirne il funzionamento e comprendere quali sono i materiali che possono esibire il fenomeno. Questo viene descritto in modo dettagliato nel primo capitolo nel quale sono anche classificate le caratteristiche dei materiali che saranno studiati.

Nel secondo capitolo è illustrata la strumentazione utilizzata ed i provini creati con PDMS e ZnS per la sperimentazione seguendo il processo di produzione descritto in letteratura.

Sarà anche provata sperimentalmente la teoria di Chandra per la quale l'emissione di luce di un materiale per effetto della meccanoluminescenza è dovuta ai dopanti e non agli atomi che compongono la struttura cristallina.

Con il terzo capitolo si apre l'analisi vera e propria, con lo studio degli elementi finiti per analizzare il fenomeno di trasferimento di sforzi fra la matrice di PDMS e la particella

inorganica di ZnS. Diversi passaggi sono stati affrontati per la realizzazione dell'analisi finale.

Innanzitutto sono rappresentate due situazioni ideali in cui la particella non risente dell'interazione dell'ambiente circostante e il caso in cui invece due particelle interagiscono completamente fra di loro per capire come cambia l'intensificazione degli sforzi. Inoltre sono analizzate altre due situazioni ideali, quali il completo trasferimento di stress dalla matrice alla particella e la situazione opposta, cioè la mancanza di interazione. Queste ultime costituiscono le estremizzazioni dei casi di interazione che possono essere presenti all'interno della matrice.

Per finire e creare una situazione più realistica vi è stato bisogno di fare una "proof of concept analysis" tenendo conto della forma e dimensioni delle particelle. Un modo per farlo è quello di raffigurare nei software quali Abaqus e Comsol un'immagine vera e propria del provino. Quindi è stato necessario un processo per trattare l'immagine, modificare la scala di grigi e ritagliare un'immagine binaria sulla quale poi fare la mesh che è stata importata ed utilizzata per l'analisi agli elementi finiti nei due software.

Infine, nel quarto ed ultimo capitolo, avendo ottenuto dei valori numerici di sforzo con l'analisi agli elementi finiti, viene proposta una teoria per il funzionamento della meccanoluminescenza di ZnS dopato e possibili vie per ottimizzarle. La teoria sarà provata poi con la parte sperimentale di produzione che richiede però ulteriori analisi per migliorare la tecnica adottata.

Table of contents

1.	Introduction.....	12
1.1.	Introduction to Semiconductor Materials.....	14
1.2.	Introduction to Luminescence.....	16
1.3.	Introduction to Mechanoluminescence.....	18
1.4.	Introduction to Piezoelectricity	20
1.5.	Property of materials under investigation.....	22
1.5.1.	Luminescence properties of ZnS	22
1.5.1.1	Elasto-Mechanoluminescence effects in doped ZnS.....	24
1.5.2.	Properties of SrAl ₂ O ₄ :Eu,Dy.....	26
	References.....	29
2.	Experimental set up.....	31
2.1.	Materials and Chemicals	31
2.2.	Composite material production.....	33
2.3.	Experimental setup.....	34
2.4.	Europium Doped crystals mechanoluminescence.....	37
	References.....	43
3.	Simulation of the behaviour of inorganic ZnS phosphors in the PDMS matrix.....	45
3.1.	Material Properties	46
3.1.1.	PDMS property	46
3.1.2.	ZnS property	47
3.2.	Modelling procedure.....	48
3.2.1.	Single particle model.....	49
3.2.1.1.	2D Geometry	49
3.2.1.2.	3D Geometry	54
3.2.2.	Two particles system geometry	58
3.3.	Complete system modelling	61
3.3.1.	Image segmentation	63

3.4.	Mesh Generation from the binary image	70
3.4.1.	Importing the .mat file in Abaqus	73
3.4.2.	Importing mesh into Comsol	74
3.5.	COMSOL.....	76
3.5.1.	Different stresses intensity with increasing number of particles.....	78
3.6.	Conclusions	81
4.	New theory for mechanoluminescence in doped ZnS	86
4.1.	Evidence in literature	86
4.2.	Shottky Diode.....	90
4.3.	Doped ZnS covered with Al.....	93
4.4.	Experimentation to prove the theory.....	97
	Conclusion	101
	References	103
5.	General conclusions and further studies.....	105

Table of figures

Figure 1.1. Representation of the energy level diagram of a semiconductor band structure where white holes are vacancies and black holes are electrons. VB is the valence band and CB the conduction band. 15

Figure 1.2. Band structure with shallow and deep levels 16

Figure 1.3. A) Absorption of energy without any defect or inclusion in the structure. B) Absorption of energy from a trap level (vacancies present). C) Radiative emission from CB to VB in the same case as A. D) Radiative emission in the same situation as B. E) Radiative emission with defects and new electronic bands due to other element inclusions. 17

Figure 1.4. Electromagnetic spectrum as a function of wavelength showing the expanded visible region. [3] 18

Figure 1.5. Piezoelectric effect in crystals. In the image on the left hand side it is possible to see the relaxed situation when no stress is applied. On the right hand side it is showed the movement of atoms after a stress is applied and the central atom moves upwards and so a difference in the polarization is generated. 20

Figure 1.6. Sphalerite and Wurtzite structure of ZnS [4] 22

Figure 1.7. Qualitative diagram to explain the difference of colour emission with the different p-dopant [16] 23

Figure 1.8. Tunnelling effect once the material is deformed by a mechanical force. 24

Figure 1.9. Bending of CB and VB and tunnelling effect of electrons with recombination after an electric field is generated. 25

Figure 1.10. Theory illustration. On the left hand side it is illustrated the bending of the CB and VB bands with tunnelling effect. The black dot have a non-radiative emission and its energy is transferred to the right hand side of the diagram where Mn energy levels are present, they absorb part of the energy, excite and when they relax the radiative emission is present. 26

Figure 1.11. Two schematic view of the monoclinic SrAl₂O₄. Reproduced from reference [13] 27

Figure 1.12. Illustration of the theory 27

Figure 2.1. Optic box with shaker, clamp and spectrometer 36

Figure 2.2. The image contains the two designed black clamps, the fibre holder and optic cable 36

Figure 2.3. SrAl₂O₄:Eu,Dy Mechanoluminescent spectrum. On the vertical axes the relative intensity is shown while on the x axes the wavelength. 37

Figure 2.4. Intensity vs time decay phenomena of ML of SrAl₂O₄:Eu,Dy. On the Y axes a relative intensity value is present while on the X axes there is the time of the experiment with different light acquisition. 38

Figure 2.5. Two frames of the video of the ML effect of the coupons with 7:3 ratio. 39

Figure 2.6. EML detection of PDMS coupons with 7:3 ratio in weight stretched with hands. 40

Figure 2.7. ML spectrum of the epoxy resin sample with 20% in weight of phosphors. 41

Figure 2.8. MoAl₂O₄:Eu,Dy luminescence peak 42

Figure 3.1. Circular ZnS particle embedded in a rectangular PDMS region. The stress is applied along the X axes and toward left while it was fully constrained on the left hand side. In this case a full stress transfer between PDMS and ZnS with indication of different magnitude of Von Mises stresses. 51

Figure 3.2. Stress-strain behaviour of ZnS elastic material in the full stress transfer between PDMS matrix and inorganic particle. 52

Figure 3.3. Circular ZnS particle embedded in a rectangular PDMS region. The stress is applied along the X axes and toward left while it was fully constrained on the left hand side. In this no contact between matrix and particle is present. Von Mises stresses are represented with the legend on the left hand side. 53

Figure 3.4. Stress and strain function of time. There should be a line at values of zero, the model is imprecise. 54

Figure 3.5. Cross-section through the 3D simulation geometry showing full stress transfer between the spherical ZnS particle in the PDMS matrix. 55

Figure 3.6. Stress versus strain plot of the ZnS inorganic particle. 56

Figure 3.7. No stress transfer representation between matrix and particle with a void formation next to the right hand side of the particle 57

Figure 3.8. Stress and strain plot vs time. There is no stress transfer so the value of stress and strain is zero. 57

Figure 3.9. Two particles with a tangent contact and full stress transfer between particles and matrix. It is clear the intensification of stresses in the contact point. 59

Figure 3.10. Stress vs strain of two particles in contact. The maximum stress is higher than in the case of single particle in PDMS matrix. 60

Figure 3.11. SEM image of a ZnS:PDMS composite taken from reference [1] 61

Figure 3.12. Manually modification of the image increasing contrast and brightness and deleting shadows. 62

Figure 3.13. Greyscale image 64

Figure 3.14. Histogram of the greyscale of the modified image. On the Y axes, the relative intensity of the colours is present. On the X axes there is the distribution of colours, with two peaks in the left and right hand side and no intensity in the middle. The left and right represent the black and white pixels while in the middle, all the shades of grey are shown. 65

Figure 3.15. Histogram of the grey scale of the unmodified image. On the Y axes, the relative intensity of the colours is present. On the X axes there is the distribution of colours, with two peaks in the left and right hand side and no intensity in the middle. The left and right represent the black and white pixels while in the middle, all the shades of grey are shown. 65

Figure 3.16. On the left hand side, it is possible to see the threshold border on the starting image and on the right hand side the binary image resulting after the segmentation. 67

Figure 3.17. Zoom on the edges of particles, they are not smooth and lot of imperfections can be seen. 68

Figure 3.18. Image obtained after the filtering process 69

Figure 3.19. Final binary image obtained after the filtering process 70

Figure 3.20. Mesh generated with Mesh2D from the binary image 73

Figure 3.21. Matlab vectorised mesh. The red dots are arrows pointing up. Each arrow is in a node of the triangulation. 75

Figure 3.22. Final image with the stress values plotted which values are seen in the legend on the right hand side. The scale is in pascal. 77

Figure 3.23. Ideal case distribution of four particles in the PDMS matrix 79

Figure 3.24. Five particles ideal case 79

Figure 3.25. More volume fraction of ZnS dispersed in the PDMS matrix 80

Figure 3.26. Random distribution with a tangent contact 80

Figure 3.6.1. Experimental analysis made in the reference [1] where performed and stress vs intensity of the ML was plotted. 83

Figure 4.1. EDS spectra of GL 25 phosphors (reproduced from Reference [7]) 87

Figure 4.2. EDS spectra of GG13 phosphor (reproduced from Reference [7]) 88

Figure 4.3. EDS spectra of GG25 phosphor (reproduced from Reference [7]) 88

Figure 4.4. ZnS powders from a TEM analysis. The ZnS particle is covered with an Al layer. 89

Figure 4.5. Metal and Semiconductor diagrams and variables. On the left hand side, the metal Fermi energy and its work function while on the right hand side the n-type semiconductor band structure is represented [10] 90

Figure 4.6. When metal and semiconductor are in contact, there is a change in the Fermi level and the bending of the energy levels. [10] 91

Figure 4.7. Barrier banding do to the electric field generated in the depletion region, Reproduced from reference [10] 92

Figure 4.8. Possible situation of the semiconductor to metal connection [10] 93

Figure 4.9. Band diagram of ZnS doped and Al [9] 94

Figure 4.10. ZnS doped and Al after the physical contact [9] 94

Figure 4.11. Reverse bias condition of ohmic contact with p-type material. Reproduced from reference 10. 97

Figure 4.12. ZnS:Mn via liquid reaction coated with Al 99

Figure 4.13. ZnS:Mn with Al via Solid state reaction 100

Figure 4.14. Orange light emission from the EML ZnS/Al powders produced by solid state reaction on the left hand side and solution processes. 101

1. Introduction

In atomic physics the electron configuration within atoms or molecules is the distribution of the electrons in their respective atomic or molecular orbitals. Electrons within these electronic configurations move independently in orbitals with velocities and spatial positions that follow Heisenberg's uncertainty principle, which gives a limitation in the precision of the determination of complementary variables of position and momentum.

According to quantum mechanics, the energy of each electron configuration can be determined. and it can be shown that electrons are able to move from one configuration to another by emission or absorption of energy in the form of photons.

Knowledge of these various configurations is essential to understand and describe not only chemical bonds that hold atoms together but also bulk material properties including distinction between metals, semiconductors and insulators.

Electrons do not occupy all the possible space, but they are confined in delocalised orbital with very precise energy levels known as quantum levels, that can be understood from the Schrödinger's equation. The separation between these quantum levels i.e. the energy gap, are portion of space are portion of space where electrons can not exist, but can move across.

In a material at zero Kelvin with no external stimulus applied, electrons will be in their lowest possible energy configuration, as understood following the Pauli principle, and the most energetic electron will be the so called Fermi level. When any kind of energy is provided to the system then electrons will start moving around the Fermi level and there is a possibility that they can occupy energy levels with a higher energy than the Fermi level. Movement of electrons generates a current and so conductive and resistive properties of materials are determined by the energy gap (or forbidden zone) that electrons need to move between. The quantum level in which the electrons have their highest energy in their ground state is referred as the valence band (VB). The unoccupied energy levels at higher energies

than the VB are known as the conduction band (CB). To have electric or thermal conduction, it is necessary for electrons jump from an occupied level in the valence band to a free one in the conduction band.

From this description it is straightforward to define materials with respective their ability to conduct.

Metals are characterized by an overlap between their VB and CB energy bands. As such there is very little or no barrier for electrons transition between these energy levels, leading to a material that is highly conductive. Even with a little energy such as the thermal one electrons can move between occupied and empty energy levels.

Insulating materials are characterized by the presence of a large energy gap between the conduction and the valence bands that electrons are not able to readily jump between bands and are confined in the valence band so that no conduction occurs in normal circumstances.

Semiconductors have finite but small energy gap between the valence band and the conduction bands. Consequently, the materials appear to be resistive in its normal state, but with sufficient energy it is possible for the electrons to overcome the energy gap and so it permits conduction. Semiconductors are classified either as intrinsic or extrinsic semiconductors. The former are the pure materials, with no defects present, whilst the latter are semiconductors that contain dopant atoms that are either electron poor or electron rich, and consequently change the band structure and therefore the electronic properties of the material.

1.1. Introduction to Semiconductor Materials.

Semiconductor materials have had a huge role in technological applications in the last century especially in the electronic sector. The history of these materials started in the 1833 with the work of Michael Faraday and continued with the theory at the bases of their mechanism in the 1878 by Hebert Hall (The Hall effect). Arguably the most significant milestone has been the development of the transistor in the 1945 lead by the team of William Shockley. From that moment on, society has made a rapid change with the development of the computer industry based mainly on silicon semiconductors. With the more recent introduction and continual development of miniaturization, semiconductor based devices have increased in their capabilities and yet changed from the large hand-held transistor of Shockley to elegant devices measured on the nanometre scale. These advances lead to the development of numerous devices including integrated circuits, tunnel diodes, MOSFET (metal-oxide-semiconductor field-effect transistor), LED (light emitting diodes), lasers, and solar cells that are nowadays ubiquitous. [1]

The action of incident photons or an applied voltage to a semiconductor material can cause electrons that lie in the valence band to be absorbed. If this energy is sufficient to overcome the band gap, electrons will be able to jump into the conduction band. This electron excitation process results in production of a hole in the valence band that is bound to the excited electron, forming a state known as an exciton. These hole-electron pairs (excitons) can be described with the same quantum physics that is used to describe a simple hydrogen atom. Therefore, excitons are attracted to each other by Coulomb forces and will therefore try to restore their initial (low energy) condition by decreasing the energy of the system. It can achieve this, if the excited electron drops to its previous low energy state by emitting a photon, i.e. via radiative emission (see (Figure 1.1)). The emission is spontaneous and the energy of the photon emitted, and therefore its wavelength if in the visible region of

electromagnetic spectra would give be observed as a colour that is characteristic of the material.

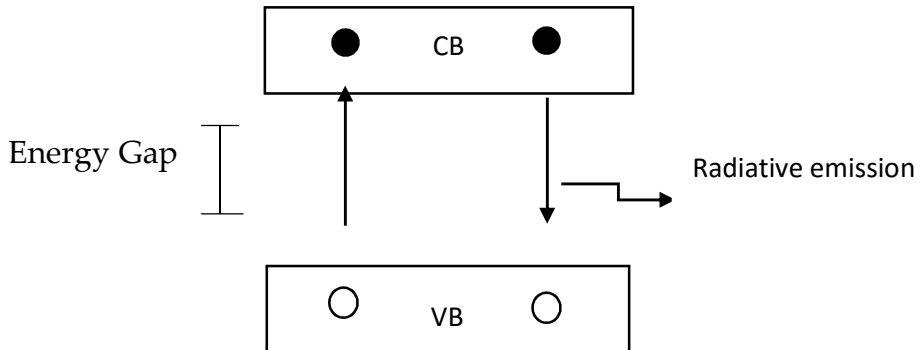


Figure 1.1. Representation of the energy level diagram of a semiconductor band structure where white holes are vacancies and black holes are electrons. VB is the valence band and CB the conduction band.

The situation becomes slightly more complicated when defects are present in the material, i.e. in extrinsic semiconductors. Defects in these materials can be produced either through vacancies in the crystal lattice or inclusion of atoms (dopants) not in the original structure of the intrinsic material. These dopant inclusions introduce new energy levels in the system between the VB and the CB levels of the native semiconductor.

Vacancies introduce so-called shallow levels, which are energy levels very close to the CB and the VB and act as trap sites for electrons and holes respectively. These trap sites have a high probability to have electrons and holes introduced by the defects itself, but they are confined to the trap levels until sufficient energy is provided to the system. On the contrary, inclusion of different dopant atoms into the lattice produces recombination centres within of the band gap (see Figure 1.2). The dopant atoms can be classified either as *n*-type and the *p*-type. The *n*-type dopants introduce extra electrons to the intrinsic material, whilst *p*-type introduce extra holes.

Moving the electrons from filled trap states to the conduction band requires much less energy (ΔE_2 , as defined in Figure 1.2) than the energy required to make the jump between the CB and the VB (ΔE_1). The inclusion of these energy levels within the energy gap is a necessary condition for some applications, such as the mechanoluminescence, as discussed below. When the excited electrons relax from the CB back down to the VB they emit energy in the form of photons. Emission in the visible portion of the electromagnetic portion of the spectra gives colours that depends on the type of dopants used and is thus different than the emission expected from the intrinsic semiconductor.

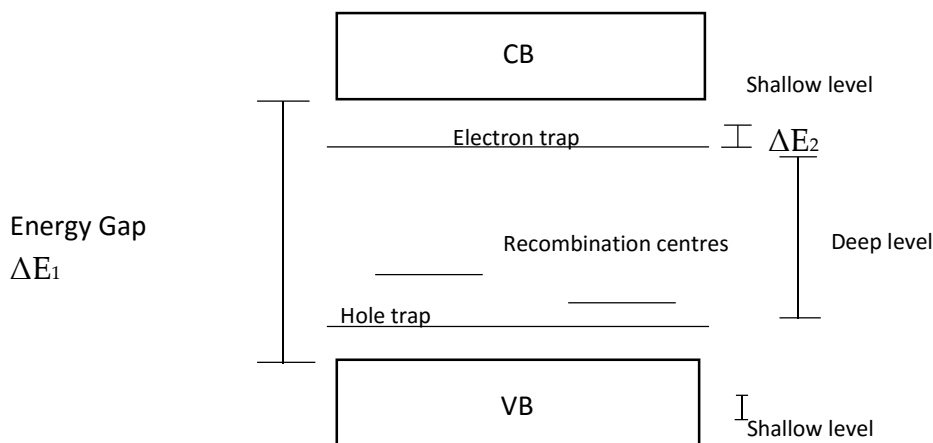


Figure 1.2. Band structure with shallow and deep levels

1.2. Introduction to Luminescence

Luminescence is a physical phenomenon that occurs when light is emitted from a material when an electron drops to lower energy states as a result of non thermal motion. There are different kinds of luminescence behaviour depending on the cause of the initial excitation, known as chemoluminescence, electroluminescence, mechanoluminescence and

photoluminescence, which are respectively produced from chemical reactions, electrical or mechanical stimuli and from an optical source. [2]

When the electrons in the conduction band relax to a less energetic state, they have to release part of their energy. This can happen following one of two mechanisms, either through a non-radiative emission, or a radiative emission. Non-radiative transitions can occur when electrons decrease their energy because of atomic motion and collisions. From the conduction band they decay to empty energy levels closer to the valence band. Radiative emission is associated with atoms emitting quantized energy in the form of photons, producing luminescence of the material. The energy released is equal to the gap of energy that they need to overcome. If the material is pure, relaxation occurs back down to the VB, or down to recombination centre energy levels if defects are present (see Figure 1.3). The wavelength emitted is related by the energy emitted and it determines the optical properties of the material.

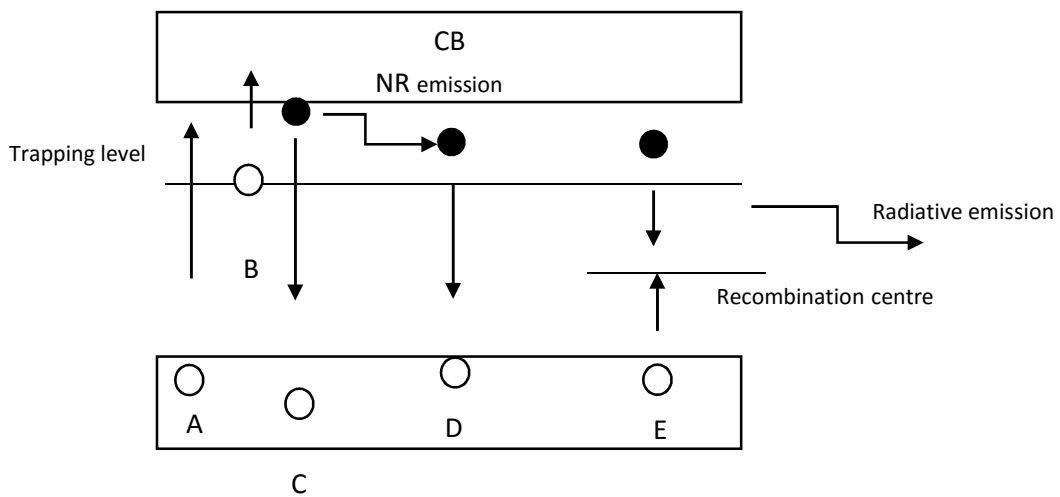


Figure 1.3. A) Absorption of energy without any defect or inclusion in the structure. B) Absorption of energy from a trap level (vacancies present). C) Radiative emission from CB to VB in the same case as A. D) Radiative emission in the same situation as B. E) Radiative emission with defects and new electronic bands due to other element inclusions.

The energy gap in any system, E, is given by $E = h \cdot v$, where $v = c/\lambda$, where c is the speed of light of the speed in vacuum (equal to $3 \cdot 10^8$ m/s), h is Planck's constant equal to 4.135×10^{-15} eV/s, v is the frequency and $\lambda (= hc/E)$ is the wavelength of the emitted photon. The different values of λ produce the well-known electromagnetic spectrum as shown in Figure 4.

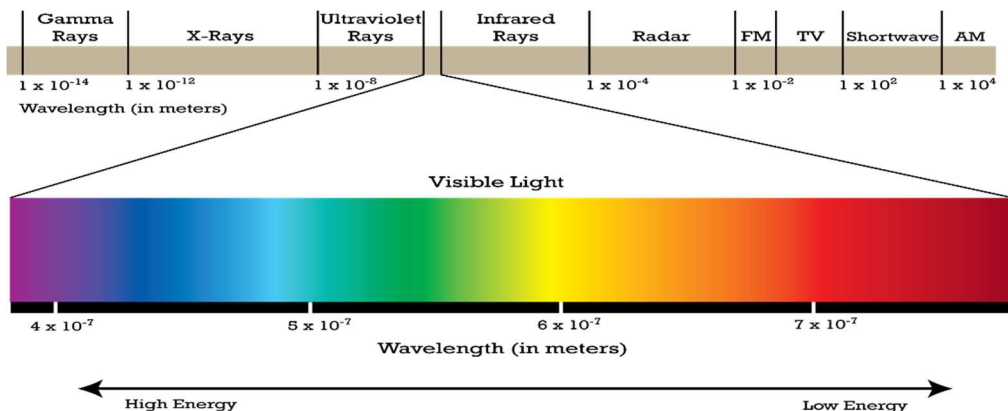


Figure 1.4. Electromagnetic spectrum as a function of wavelength showing the expanded visible region. [3]

In this thesis, materials that emit in the visible region of the electromagnetic spectrum range will be taken into consideration.

1.3. Introduction to Mechanoluminescence

Luminescence caused by any mechanical stimulus on a material is called mechanoluminescence (ML). This is the modern name given to an older term associated to a phenomenon, first described in the 17th century, and known as triboluminescence. The first known written description of ML was written by Francis Bacon in 1605 in his work "*Of the Proficiency and Advancement of Learning, Divine and Human*" where he stated that "*hard sugar being nimbly scraped with a knife would afford a sparkling light.*" By the end of the 1700s, a

number of minerals and pottery materials were shown to exhibit ML. ML has also been observed in natural phenomena, for instance light emission associated with rock failure in mines and earthquakes have been reported for several centuries. [5]

More recently, research into ML phenomena has gained considerable interest, helped by the development of spectrometers for the detection of the triboluminescence in the latter half of the 20th Century. Over the last few decades, Chandra has made a significant contribution to the study of ML phenomenon. Mechanoluminescent materials act as transducers so they convert the applied mechanical energy to electromagnetic energy. Therefore, mechanoluminescence can be sub-divided into different classes depending on the response of the materials being mechanically deformed [4]. ML materials can therefore be defined as being produced by plastic (PML), elastic (EML) or by fracture (FML) deformation. In FML, the luminescence is generated due to the creation of new surfaces during the rupture of a solid, whilst PML is produced during plastic deformation, and finally the EML is produced during elastic deformation. [6]

The number of solid materials that are EML and PML is very small compared with the large number of FML materials [7]. In this thesis, EML materials are considered the most promising among the ML materials, since it is the only mechanism that is repeatable in mechanical cycling. In particular, between the large number of mechanoluminescent materials discovered to date, attention has often focussed on those that exhibit intense luminescence, such as ZnS:Cu, ZnS:Mn. [8]

Nowadays these materials have received a lot more attention for their possible application in the stress sensing, as used for example in crack monitoring. ML can provide a self-indicating method of monitoring the microscopic and macroscopic processes occurring during deformation and fracture of solids. It can also be used for measuring the crack velocity, fracture initiation time, local stress and temperature near a moving crack-tip.

Measurements may also be useful for non-destructive testing of solids. [4]

1.4. Introduction to Piezoelectricity

Piezoelectricity is the property exhibited by some crystals to polarize and to generate a potential difference when they are mechanically deformed, known as the direct piezoelectricity effect. Conversely, these crystals can elastically deform when a current is applied to them and known as the inverse piezoelectric effect. While the direct effect is generalized to the whole material, the inverse effect is seen only along one crystallographic direction and the resulting deformation is on the nanometre scale.

Piezoelectricity was discovered for the first time in the 1880's by Pierre and Paul Curie when they discovered first the direct effect in quartz and lately the inverse effect. [9]

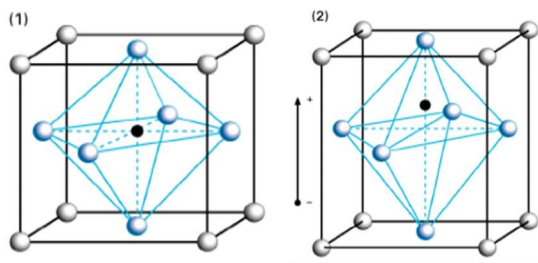


Figure 1.5. Piezoelectric effect in crystals. In the image on the left hand side it is possible to see the relaxed situation when no stress is applied. On the right hand side it is showed the movement of atoms after a stress is applied and the central atom moves upwards and so a difference in the polarization is generated.

The direct piezoelectric effect is present in almost all crystalline materials that have no centre of symmetry. The crystalline structure is constituted by microscopic electric dipoles. When no perturbation is applied to them, these dipoles are arranged in such a way that the faces of the crystal have the same electric potential and so an electrical neutrality is maintained. When a compressive force is applied, the structure is deformed and the electric neutrality of the material is lost, so a face is charged negatively and the opposite face positively. If there is a tensile force, the charges of the faces are inverted with respect to the previous

situation. The crystal acts therefore as a capacitor and if the two faces are connected to an external electric circuit, then a current is registered. [9]

By contrast, for materials that exhibit an indirect piezoelectric effect, when a potential difference is applied to the material, depending on sign of the applied field, the crystal structure expands or contracts along an axis. The volumetric expansion is directly linked to the electric stimulation and it will be discussed in the last chapter of the thesis with the introduction of constitutive equations.

These materials are characterized by different value of the so called piezoelectric constants that relates the strain developed and the applied electric field:

$$D_{ij} = \frac{\text{strain developed}}{\text{applied electric field}}$$

Equation 1.1. Piezoelectric constants that relate the strain to the electric field.

They depend on the direction of the plane (i.e. i and j) in which the force is applied with respect to the direction of the generated electric field. The most significant parameter is D_{33} , as it is the largest, is directly related to the electric field in the same direction in which the force is applied.

The charge density, Q , is related to the applied stress is given by $Q = \sigma \cdot D_{33}$ from which the piezoelectric field generated, $E = Q/\epsilon_0$, can be determined.

A generated electric field does not take into account the intrinsic properties of the material; therefore, it is only correct for the external field generated around the crystal. In the inner part of the crystal, the medium has to be taken into account, and so the field will be reduced since the dielectric constant has a value higher the one in vacuum.

1.5. Property of materials under investigation

1.5.1. Luminescence properties of ZnS

ZnS is an undoped semiconductor composed of 1:1 ratio of Zn^{2+} and S^{2-} ions, which forms a crystalline solid with two polymorphs - Wurtzite and sphalerite. The Wurtzite structure has a hexagonal close pack (HCP) structure, whilst the sphalerite structure is a cubic close packed (CCP) (see Figure 1.6). [10]

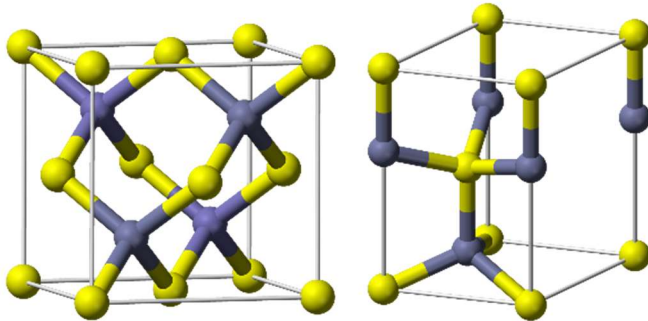


Figure 1.6. Sphalerite and Wurtzite structure of ZnS [4]

The Zn^{2+} are the yellow dots while the S^{2-} are the blue dots. [11]

ZnS is a direct band gap semiconductor with a band energy gap of either 3.64 eV for the sphalerite structure, or 3.74 eV for the Wurzite structure [10]. These band gaps would both produce blue light emission with wavelengths of 340.7 nm and 331.68 nm, respectively. In practice experimental measurements, the emission peak of the ZnS is around 450nm for either structure [11-12] which means that defects are present in the ZnS structure causing formation of energy levels within the band gap of the system. These defects have been

shown to be the result of Zn vacancies leading to hole trap states close to the VB of the ZnS, and S vacancies forming electron trap states close to the CB. [13]

The ZnS can also be optically activated when a small concentration of Ag^+ , Cu^{2+} or Mn^{2+} ions are added to the crystal. These dopants change the emission spectra of the ZnS, because the impurities provide new recombination energy levels within the band gap [10]. The dopant metal ions substitute the Zn^{2+} in the crystal lattice giving a slight distortion to the lattice itself. Given their relative position in the periodic table with respect to Zn, means that Cu, Mn and Ag dopants are electron poor with respect to the Zn, so they bring new acceptor levels above the valence band i.e. they are *p*-type dopants.

In the case of *n*-doped materials, dopants such as Al^{3+} , which has more electrons than the host Zn forms a new energy state full of electrons close to the CB. Experiments on doped ZnS have shown that Ag^+ dopant gives a blue emission colour, Cu^{2+} dopant gives a green colour and Mn^{2+} dopant a yellow colour, it is therefore possible to construct a schematic energy diagram of doped-ZnS as shown in figure 1.7. [14] [15]

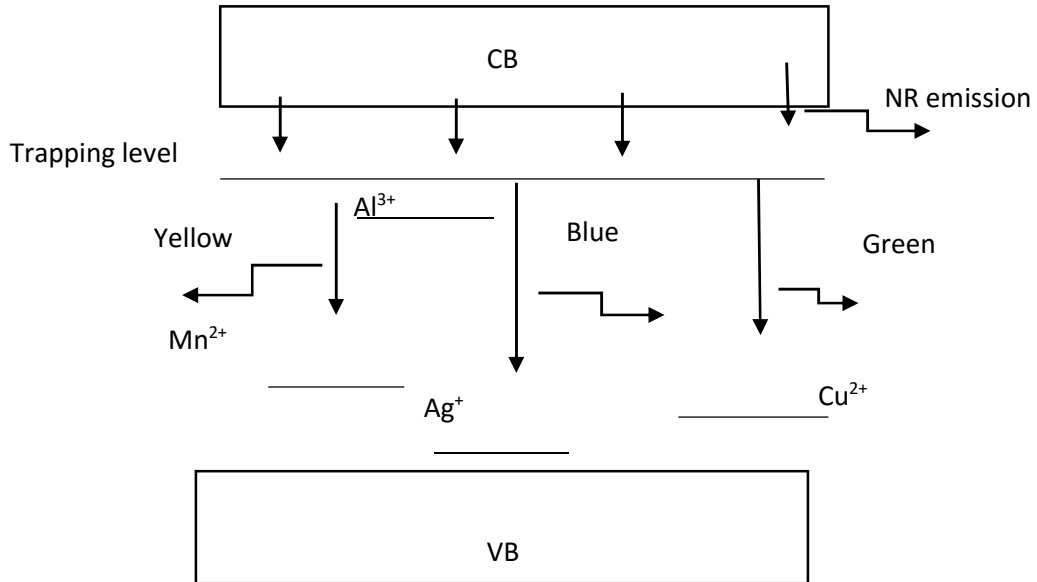


Figure 1.7. Qualitative diagram to explain the difference of colour emission with the different *p*-dopant [16]

1.5.1.1 Elasto-Mechanoluminescence effects in doped ZnS

The mechanoluminescence emission of doped ZnS is believed to occur through one of two unproven mechanisms, either due to electrostatic interactions between dislocation and the filled electron traps, or due to a piezoelectric effect that induces electron detrapping. These are two mechanisms proposed by Chandra in [17] that are not yet proven.

- 1- In the electrostatic model dislocation defects in the crystal (due to the dopant atoms) are distorted due to an applied elastic deformation. The recombination bands associated with the dopant atoms are therefore bent (see Figure 1.8), which causes an electric field to be generated associated with the bending of the valence and conduction bands. This provides the electrons present in the trap states a higher probability to tunnel into the conduction band. Electrons that loose energy from the CB by recombination with holes in the recombination levels do so by radiative emission, emitting light in the visible region [17].[18] (Figure 1.8)

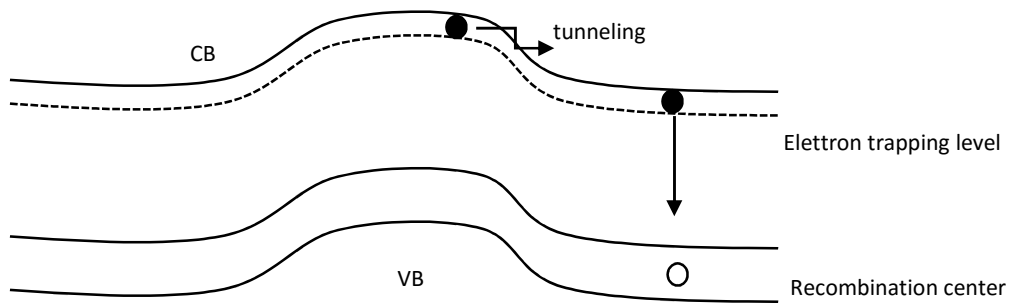


Figure 1.8.Tunnelling effect once the material is deformed by a mechanical force.

2. The second theory is thought to work since ZnS is a non-centrosymmetric crystal, [19] and consequently is a piezoelectric active material. The magnitude of the local dielectric constant of ZnS depends on the distance from the distance from the dopant atoms, with the highest values closest to these defect atoms. The upshot of this

variation in dielectric constants is a gradient in the electric field within the sample causes a slope in the CB and VB energy levels in the regions near the dopant atoms. The electrons in the trapped states near the dopant atoms can therefore easily tunnel to the CB level. These excited electrons can then relax via non-radiative emission either down to the VB or the recombination energy levels (see Figure 1.9).

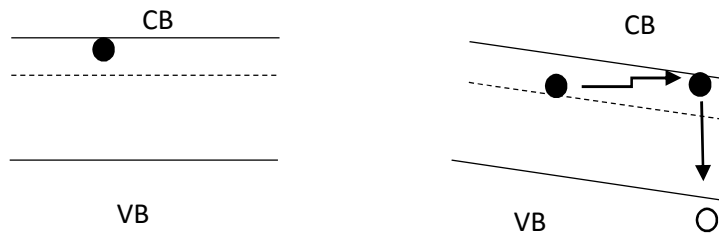


Figure 1.9. Bending of CB and VB and tunnelling effect of electrons with recombination after an electric field is generated.

Some of this non-radiative energy can excite electrons in the dopant atoms to higher energy levels within the band gap, i.e. between the CB and the VB levels, that were previously empty (since the dopants are *p*-type donors) (see Figure 1.10). Relaxation of these excited electrons back to their ground state is radiative with wavelengths in the visible region. This mechanism is seen to be consistent with loading and unloading of mechanical stress on the piezoelectric material.

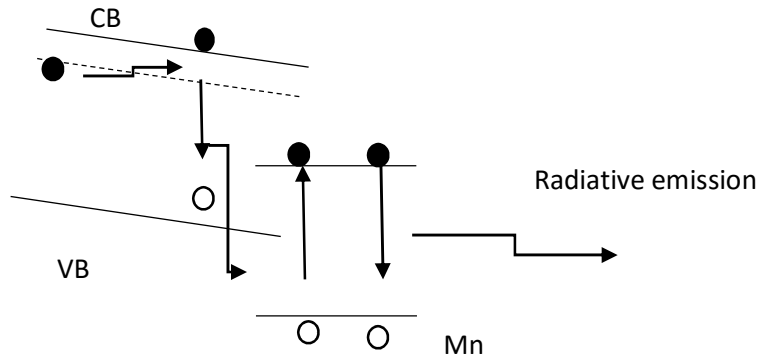


Figure 1.10. Theory illustration. On the left hand side it is illustrated the bending of the CB and VB bands with tunnelling effect. The black dot have a non-radiative emission and its energy is transferred to the right hand side of the diagram where Mn energy levels are present, they absorb part of the energy, excite and when they relax the radiative emission is present.

1.5.2. Properties of SrAl₂O₄:Eu,Dy.

Doped strontium aluminate, SrAl₂O₄:(Eu,Dy), is a crystalline solid possesses a monoclinic unit cell, with a spinel structure of the kind AB₂O₄. The structure consists of a CCP array of O²⁻ ions, with the A cations (Sr) occupy one-eighth of the tetrahedral holes and the B cations (Al) occupy half the octahedral holes [10]. As is also seen with doping in ZnS, only when doped with europium and dysprosium does display SrAl₂O₄ strong ML. Since Sr²⁺ and Eu²⁺ or Dy²⁺ have some very similar atomic radii, doping with this metal causes very little distortion of the crystalline structure.

As seen for ZnS doping of the intrinsic structure is the necessary condition to induce mechanoluminescence.

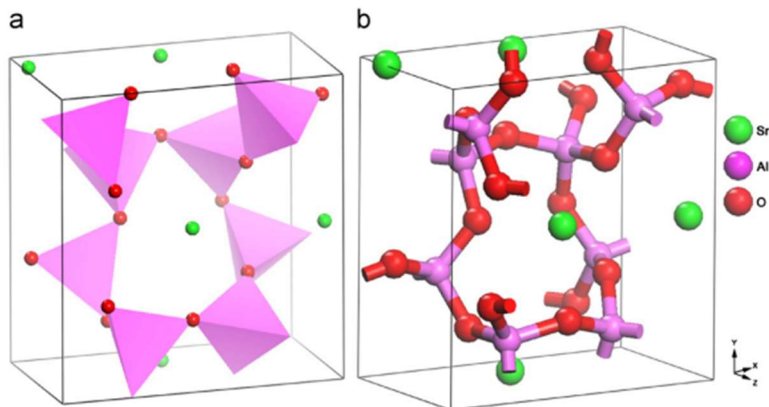


Figure 1.11. Two schematic view of the monoclinic SrAl_2O_4 . Reproduced from reference [13]

The mechanoluminescent phenomenon in SrAl_2O_4 has been described mechanistically by Jha and Chandra [20]. Their theory also relies on changes in the dielectric constants around the dopant atoms compared to the pure SrAl_2O_4 . Consequently, an applied force causes a local piezoelectric field in the crystal that is larger closest to the dopant atoms compared to the pure matrix. The induced electric field causes bending of energy bands allowing electrons to move from the trap states to the CB either by tunnelling or due to kinetic effects due to the temperature. The electrons in the CB can be captured by the dopant ions which then relax to lower energy dopant energy levels via radiative energy loss to give luminescence.

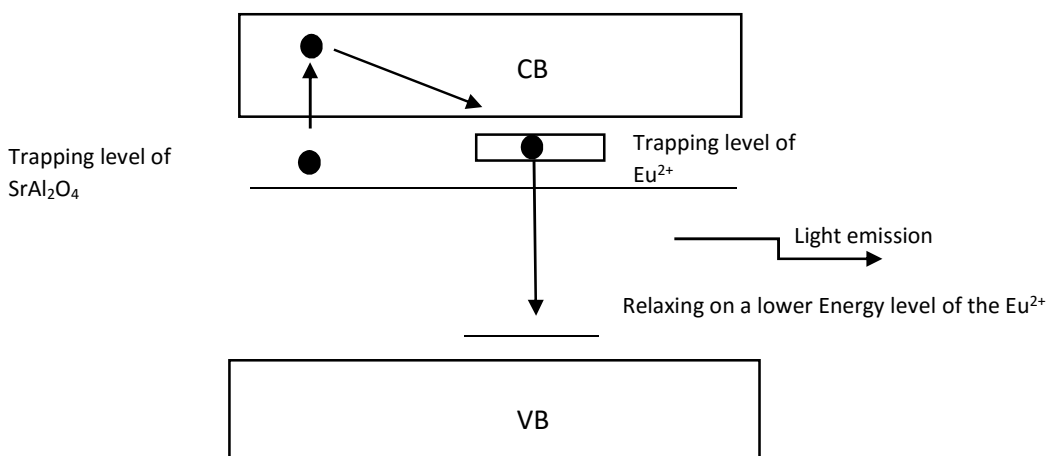


Figure 1.12. Illustration of the theory

The related molybdenum aluminate, $\text{MoAl}_2\text{O}_4:(\text{Eu},\text{Dy})$, has the same crystal structure as the $\text{SrAl}_2\text{O}_4:(\text{Eu},\text{Dy})$, with the Mo replacing the Sr in the lattice. Although both compounds are ML active, $\text{SrAl}_2\text{O}_4:(\text{Eu},\text{Dy})$ produces persistent ML, whilst $\text{MoAl}_2\text{O}_4:(\text{Eu},\text{Dy})$ displays instantaneous ML.

References

- [1]. Lidia Łukasiak and Andrzej Jakubowski. History of Semiconductors. *Journal of telecommunications and information technology* 1/2010.
- [2] <https://en.wikipedia.org/wiki/Luminescence>
- [3] <http://blog.luxexcel.com/printed-optics/light-spectrum/> (date of consultation)
- [4] B. P. Chandra. Mechanoluminescence.. *Luminescence of solids* pp 361-389 copyright 1998. Editors D.R. Vij. Editor Affiliations department of Physics Kurukshetra University
- [5] B.T Brady & Glen A. Rowell. Laboratory investigation of the electrodynamics of rock fracture. *Nature* vol 321. 29 May 1986
- [6] B. P. Chandra and A. S. Rathore. Abstract from Classification of Mechanoluminescence. Volume 30, issue 1995 Pages 885–896
- [7] B.P. Chandra, Disha Satya Vihar, Vidhansabha-Chandrakhuri Marg. Mechanoluminescence of Nanoparticles Academy of Research and Education, Disha Institute of Management and Technology. Raipur 492101 (C.G.), India
- [8] Leelachao, S., Muraishi, S., Sannomiya, T., Shi, J., & Nakamura, Y. (2016). Correlation of triboluminescence and contact stresses in ZnS:Mn/polymeric matrix composite. *Journal of Luminescence*, 170, 24–29.
- [9] Lecture and note of Cinzia Cristiani. Associate professor. Dipartimenti di Chimica, Materiali ed Ingegneria Chimica “G.Natta” Politecnico di Milano
- [10] Inorganic Chemistry Shiver & Atkins fifth edition. Atkins, Overton, Rourke, Weller, Armstrong. Published in 2010 in Great Britain by Oxford University Press.
- [11] https://en.wikipedia.org/wiki/Zinc_sulfide
- [12] S.Ummartyotin et. Al. Synthesis and Luminescence properties of ZnS and Metal (Cu,Mn) doped ZnS ceramic powder. *Solid State Sciences* Volume 14, Issue 3, March 2012, Pages 299–304
- [13] Wang, W., Huang, F., Xia, Y., & Wang, A. (2008). Photophysical and photoluminescence properties of co-activated ZnS:Cu,Mn phosphors. *Journal of Luminescence*, 128(4), 610–614.

- [14] P. Prathap, N. Revathi, Y.P.V. Subbaiah, K.T.R. Reddy, R.W. Miles, *Solid State Science*. 11 (2009) 224.
- [15] K. Manzoor, S.R. Vadera, N. Kumar, T.R.N. Kutty, *Applied Physics Lett.* 84 (2004) 284.
- [16] Krishnan, S. (2015). Mechanoluminescent and Phosphorescent Paint Systems for Automotive and Naval Applications.
- [17] Tiwari, R., Dubey, V., & Chandra, B. P. (2014). Exact model for the elasto mechanoluminescence of ii-vi phosphors, 19, 25–38.
- [18] B.P. Chandra, C.N. Xu, H. Yamada, X.G. Zheng, J. *Journal of Luminescence*. 130 (2010) 442.
- [19] Hao-Ying Lu, Sheng-Yuan Chu, Soon-Seng Tan. The characteristics of low-temperature-synthesized ZnS and ZnO nanoparticles. Volume 269, Issues 2–4, 1 September 2004, Pages 385–391
- [20] Jha, P., & Chandra, B. P. (2013). Impulsive excitation of mechanoluminescence in SrAl₂O₄: Eu, Dy phosphors prepared by solid state reaction technique in reduction atmosphere. *Journal of Luminescence*, 143, 280–287.

2. Experimental set up

The motivation for this project was the work by Soon Moon Jeong et Al. [1] who used ML phosphors embedded in a PDMS elastomer matrices to generate light through mechanical deformation.

They produced the so called ACEL devices consisting of ZnS:Mn and ZnS:Cu embedded in the PDMS. These devices produce EML when deformed with a very low mechanical stress, with values lower than the MPa. Moreover, they produced road like PDMS coupons so that stream of gas was sufficient to make them vibrating and show mechanoluminescence. They also found a correlation between frequency of oscillation and the spectrum. [1]

The current work aimed to study the fundamental principles behind these intriguing experimental ML studies, and specifically determine how the luminescence intensity is linked to the stress applied and how the stress is transferred between the polymeric matrix and the inorganic particles. The mechanoluminescent phosphors used in this thesis are micro sized particles. They emit visible light when pressure is applied to them either by grinding or compression of the powders.

2.1. Materials and Chemicals

Polydimethylsiloxane (PDMS) belongs to the group of polymeric viscoelastic organosilicon compounds, and is a widely used elastomer that is optically transparent, chemically inert, non-toxic and non-flammable. The PDMS used in this project was Dow-Corning Sylgard 184 purchased from Sigma Aldrich. Sylgard 184 is sold as a two part kit consisting of a

silicon-based oligomer base and a curing agent which must be mixed in the appropriate ratio (10:1 by weight of base:curing agent) and allowed to cure to form the solid elastomer. Curing times differ depending on the temperature and drop from ~48 hours at room temperature to ~10 mins at 150 C [2].

The Sylgard 184 elastomer has the ideal elastic properties required for this thesis. When the ML phosphors are mixed with the PDMS, the composite becomes opaque taking on the native colour of the powders, but remains mechanically flexible.

Almost all the doped ZnS systems used in a majority of the relevant papers in the literature, are the phosphors known commercially as GG13, GG25 and GG45 and manufactured by GTP Corporation. Those phosphors are the most promising because a very little stress is sufficient to cause the ML behaviour.¹ However, it was not possible to find a distributor who would supply suitable quantities of these materials. [3]

As an alternative ZnS:Mn, commercially known as GL25, was bought from Phosphor Technology Ltd. (UK). As discussed in the results section below this phosphor, ultimately did not meet the initial expectations and was not used in subsequent experiments in PDMS composites.

Though, this phosphor, was not suitable for our goal. Only through scratching and grinding mechanoluminescence appears, not when embedded in the PDMS and mechanically pulled. This is due to the fact that the stress required to have mechanoluminescence is too high and not reachable when embedded in the matrix. When scratched with a glass rod, it is possible to see clear sparkles of orange light.

In addition, SrAl₂O₄:(Eu,Dy) was purchased from Osram Sylvania. The received powders, have average diameters of several microns, but unlike the ZnS:Mn phosphors they exhibit permanent luminescence. This means that once excited by mechanical straining, the decay time of the luminescent intensity is very slow. Moreover, when irradiated with UV light bright luminescence intensity is observed from the powders.

$\text{MoAl}_2\text{O}_4:(\text{Eu},\text{Dy})$ was taken from Blanche Jamie, a PhD student at the Heriot-Watt university who bought it from Eli-Chem Resins (U.K) Ltd.

Moreover, the procedure to product ZnS doped with Mn, Cu, and Mn,Cu described in [4] was followed with three methods and it will be described in the last chapter but no mechanoluminescence results was obtained when grinding or indenting with a glass rod.

2.2. Composite material production

In the literature, [5-10] a standard procedure has been followed where a weight ratio of 7:3 ZnS:PDMS mixture is used. The process for the production of the ML test samples was to gently stir the phosphors powders together with the Sylgard 184 base:curing agent mix (10:1 by weight) until the system was homogeneously mixed. The highly viscous fluid was poured into an aluminium pan ~5 cm square and then degassed under vacuum (in a vacuum oven) at room temperature for ~20 minutes to remove any trapped bubbles. The ~1mm thick composite was then thermally cured at 100 C to permit the PDMS to crosslink properly.

However, it was found that it was not always possible to achieve complete curing of the Sylgard 184 for all the phosphors when mixed at the desired 7:3 ratio (phosphor:elastomer). The composites formed with ZnS and ZnS:Mn lost both flexibility and elasticity, forming almost brittle materials that failed at very low strain and contained a large numbers of holes due to the air that was not able to diffuse completely. To achieve any degree of toughness and elasticity, it was necessary to mix at a weight ratio of 1:2 ZnS : PDMS. For the $\text{SrAl}_2\text{O}_4:(\text{Eu},\text{Dy})$ and $\text{MoAl}_2\text{O}_4:(\text{Eu},\text{Dy})$ phosphors it was possible to obtain the desired 7:3 ratio composites with useable elastic properties. The reason of the difference in the behaviour is thought to be related to the particle size its distribution. The phosphors made

in house (by Laura English, Heriot-Watt University) [11] do not have a homogeneity in the size distribution and are have on average a larger size than the commercially sourced phosphors.

2.3. Experimental setup

Since the idea is to perform optical analysis under stress conditions, different tools are needed

- A mechanical shaker in order to mechanically deform the material during stress cycles
- A clamp to hold the sample
- A spectrometer and an optical fibre to collect the emitted light and analyse the wavelength
- An optical dark box to perform measurements without any interference from the environment around.

The mechanical shaker model K2007E01 was purchased from Modal Shop from the USA and it is a useful device for frequency depending loading.

The maximum applicable force during testing is 31 Newton and it is needed a direct current supply from any 12-21 volt. The frequency input was given by a frequency generator downloaded on a smartphone where low frequency (such as 1 to 5 Hz) are permitted.

Moreover, it doesn't allow stress to be measured, it has to be calculated with the strain applied to the material.

In this thesis no results are reported where the frequency dependency is considered, but it is used to apply very low stresses to the PDMS coupons. It is possible to change the

frequency of the oscillation with a frequency generator and study how the material reacts to different situations. Moreover, it has a support to hold to the optical board and being stable.

Two clamps to hold the sample were created, one to be screwed in the shaker and the other one that consist in the steady clamp with the mechanical support. They were designed in aluminium and fabricated from the mechanical engineering department of the university.

To avoid any kind of interference with the external environment and especially with the light, components to create an optical board from Thor Labs were bought that can contain the shaker, the clamps and the spectrometer. So when performing the experimentation everything is sealed in complete darkness.

An optical fibre (QP1000-2-UV-BX, 1mm core diameter), an Ocean Optics Flame UV-vis spectrometer (model FLAME-S-UV-VIS) and Spectra Suite software were purchased from Photonic Solutions (UK). The Flame spectrometer has a wavelength range of 200-850 nm with a 1.5 nm resolution. A 5 mm UV/vis collimating lens with a 200-2000 nm spectral range, and a focal length of 10 mm, was fitted to the end of the fibre optical cable to maximise the light collected by the spectrometer.

The experimental set up can be seen in Figures 2.1 and 2.2.

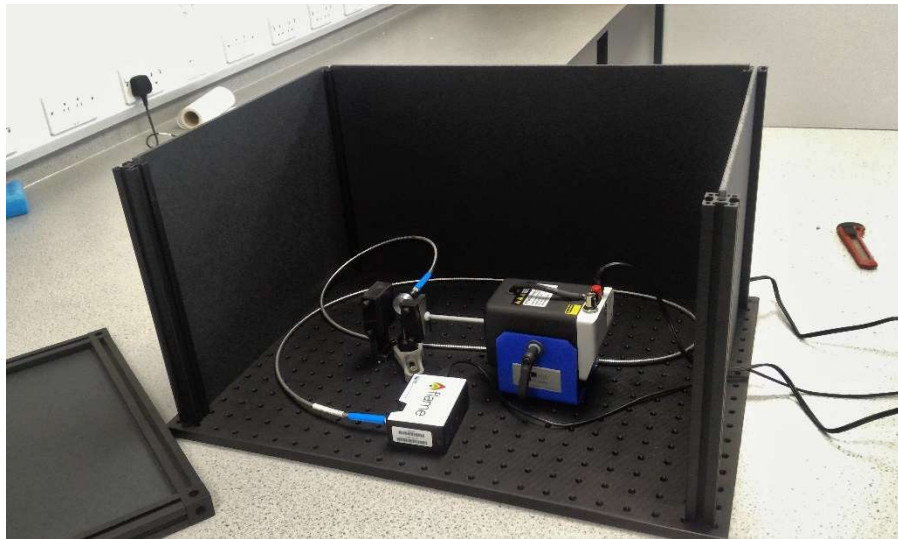


Figure 2.1. Optic box with shaker, clamp and spectrometer

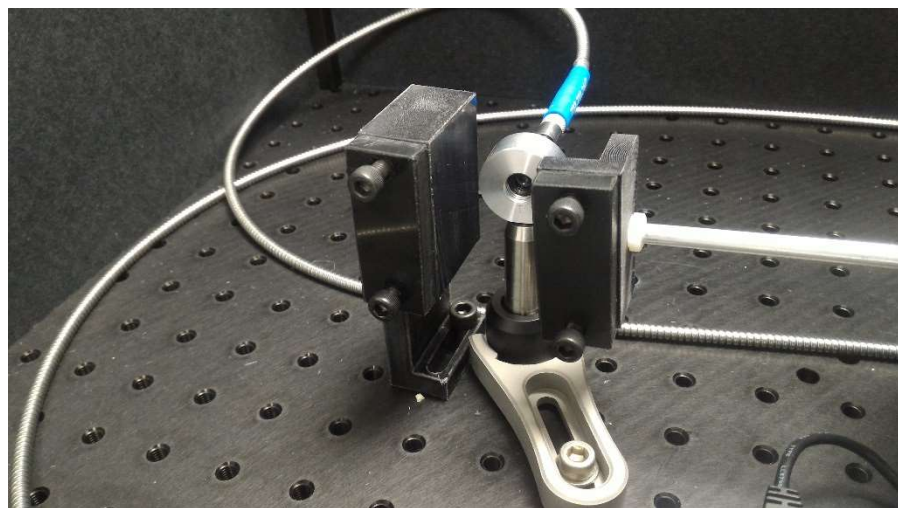


Figure 2.2. The image contains the two designed black clamps, the fibre holder and optic cable

In figure 2.1 and 2.2 the experimental equipment is shown and it is possible to see the shaker, the flame series spectrometer, the optic cable the clamps and the optical box.

2.4. Europium Doped crystals mechanoluminescence

Spectra Suite software was used to collect spectra after subtracting background noise levels, from a spectra obtained of the ambient light levels before any luminescent measurements were taken. This background spectrum was automatically subtracted from the subsequent measurements by the Spectra Suite software. Since the ML observed in these systems was found not to be very intense in order to maximise the signal to noise ratio in the experiments, measurements were performed over extended exposure times in addition to using the internal multiple integration feature in the software. For the ML detection of SrAl₂O₄:Eu,Dy typical measurements used an exposure time was of a minute and a half with averaging over 4 spectra. Given these long data collection times, it was not possible to observe time dependent features at time scales of less than a few minutes.

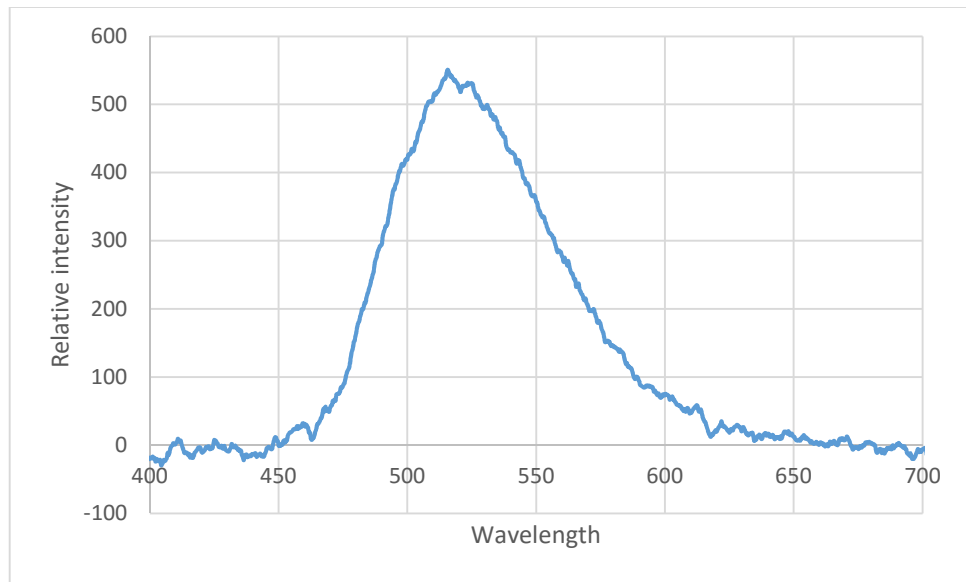


Figure 2.3. SrAl₂O₄:Eu,Dy Mechanoluminescent spectrum. On the vertical axes the relative intensity is shown while on the x axes the wavelength.

It is possible to see a peak around a wavelength of 520 nm with a relative high intensity.

Since this is a permanent luminescent material, the study of the decay of the intensity versus the time is interesting.

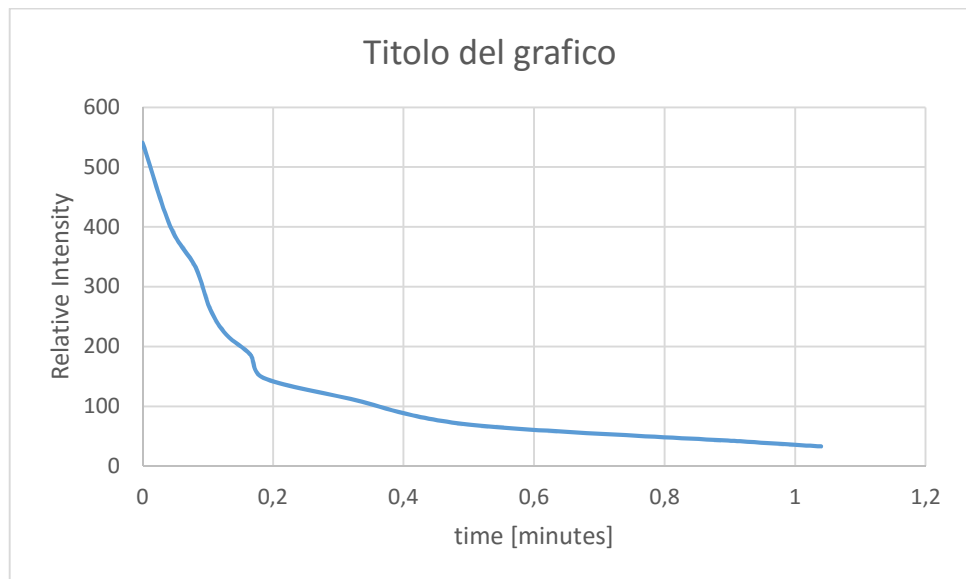


Figure 2.4. Intensity vs time decay phenomena of ML of $\text{SrAl}_2\text{O}_4:\text{Eu},\text{Dy}$. On the Y axes a relative intensity value is present while on the X axes there is the time of the experiment with different light acquisition.

What is visible in the graph above is that the intensity rapidly decreases reaching after a certain time an asymptotic value at very low intensity. This explains why these ML phosphors are known as 'persistent'.

To prove the theory of Chandra explained in [10] about the mechanism of mechanoluminescence, it was needed to make a comparison between $\text{SrAl}_2\text{O}_4:\text{Eu},\text{Dy}$ and $\text{MoAl}_2\text{O}_4:\text{Eu},\text{Dy}$. As a matter of fact, as it was previously explained, the theory of Chandra affirms that the ML wavelength properties depends only on the dopant, not on the structure. The piezoelectric structure is needed to generate an electric field and to give electrons to the dopant materials, but it does not influence the emitted wavelength.

So with the shaker, a ML analysis was performed on MoAl₂O₄:Eu,Dy. This material is different from the strontium doped one because its mechanoluminescence is not permanent but instantaneous.

Two samples were made, a 7:3 ratio and a 1:2 ratio of phosphor:PDMS. What is possible to see is that in neither case is EML observed under oscillatory mechanical strain of 10% (That is the maximum value of strain applied) produced by the shaker at frequencies between 1 and 8 Hz. This means that the stress transmitted to the powders it is not high enough.

In the low dense coupon, it is possible to see EML when stretched with hands, so when a higher stress is applied to the material. In the high volume fraction sample, the same result is obtained but at lower stress and the intensity obtained is higher.

So the volume fraction is fundamental to reduce the EML threshold and to give emission of light at lower stresses and to increase the intensity itself.

Moreover, what is seen during the bending process is that the higher intensity is along the line where the coupon is clamped and in the case of fracture the intensity is very high.

The video of the EML phenomena of MoAl₂O₄:(Eu,Dy) was recorded with a smartphone placed inside the optical black box while stretching by hand the material.

Some frames are extracted from it using windows movie maker.

The two pictures below show the results, the green emission that is characteristic of the Europium at 520 nm.



Figure 2.5. Two frames of the video of the ML effect of the coupons with 7:3 ratio.

It was possible to obtain a spectra of the coupons that exhibit mechanoluminescence capturing the light emitted after a certain number of cycles. The result is not precise and the peak is too broad because a sharp peak around 520 nm was supposed to appear.

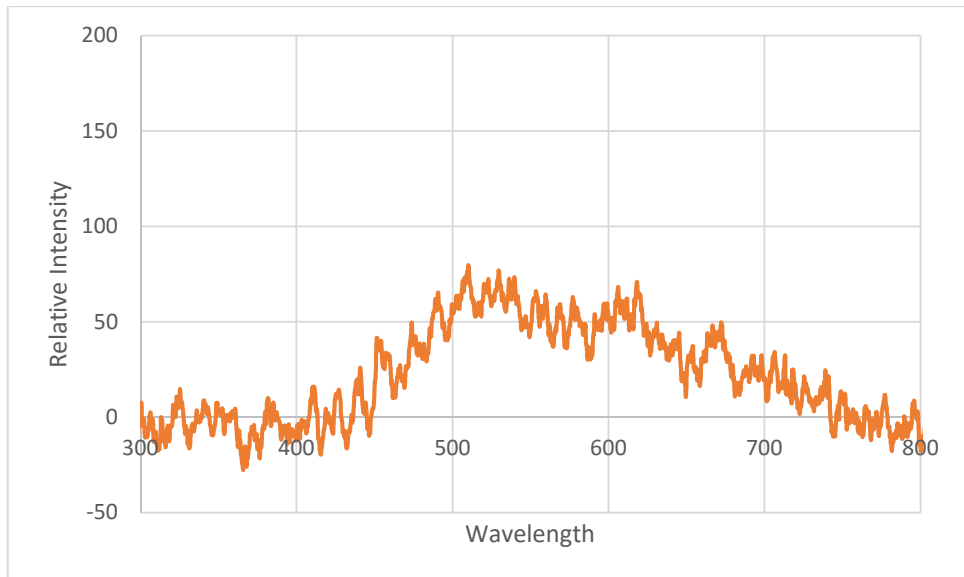


Figure 2.6. EML detection of PDMS coupons with 7:3 ratio in weight stretched with hands.

A better spectrum from the EML phenomena was obtained in a slightly different way. Coupons were made by Jamie Blanche, a PHD student from Heriot-Watt university who made an epoxy resin matrix acquired from Eli-Chem Resins (U.K) Ltd, Surrey, with good UV stability and minimal polymer shrinkage during curing in which the $\text{MoAl}_2\text{O}_4:\text{Eu},\text{Dy}$ was added at 20% ratio by weight of the matrix. The samples have completely different characteristic, they are not anymore elastic like the PDMS ones, but they are stiff and rigid. For the test a hydraulic press was used to give the right amount of stress to see the phenomena. The values around which it is possible to start seeing the EML is on the order of 10-15 kg/cm².

The spectrum was detected with the fibre optic cable and the Spectra Suite software and it is shown in Figure 2.3.

The exposure time to detect the EML phenomenon lasted until the brittle failure of the sample, so it is approximatively one minute. During this time repetitive loading are applied to the material with the hydraulic press and it is possible as explained in a paper done by Jamie and me [12] to see an instantaneous increase of luminosity at each increasing of loading.

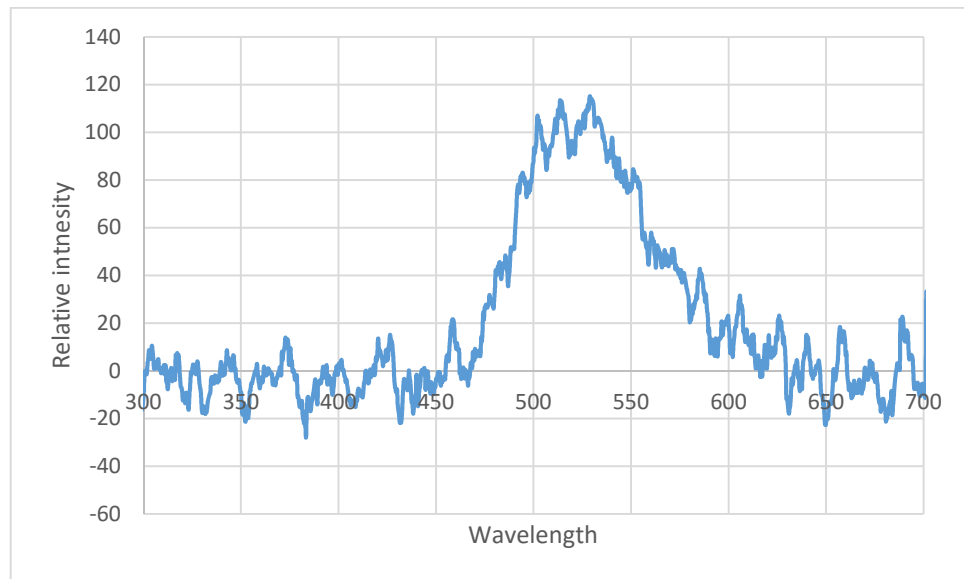


Figure 2.7. ML spectrum of the epoxy resin sample with 20% in weight of phosphors.

It is possible to analyse the two graphs and to compare them. It is visible that in the second case a narrower peak is obtained due to the higher intensity emitted from the sample. It is hard though to make a real comparison because of the different matrixes used in the two cases and the different percentage of material used.

To obtain a spectrum to prove Chandra theory, [10] the sample was exposed to light from an UV source for 10 minutes and the emission of light afterwards was persistent.

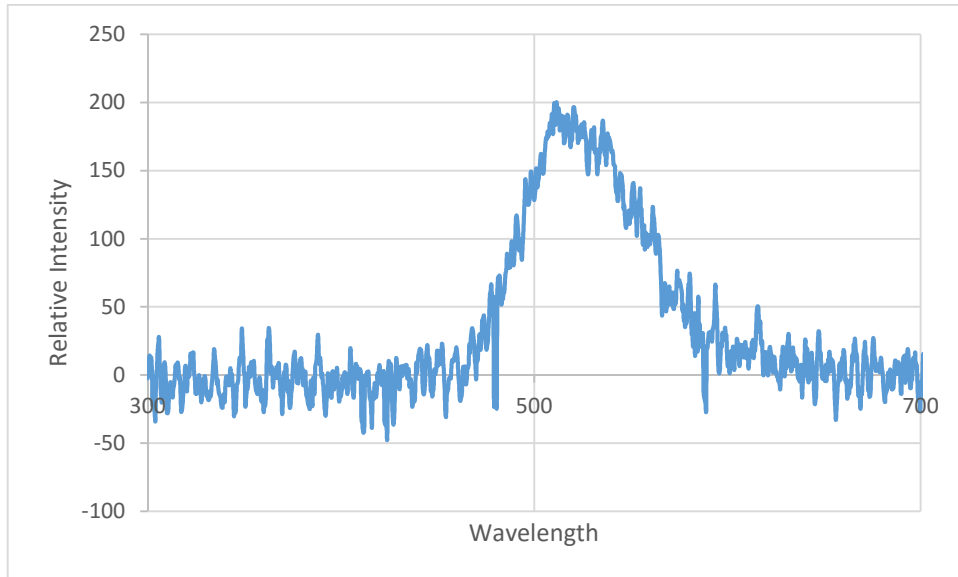


Figure 2.8. $\text{MoAl}_2\text{O}_4:\text{Eu},\text{Dy}$ luminescence peak

We can clearly see again the peak at 520 nm so it implies that as stated in [10] the emission is only due to the Europium and not to the crystalline structure around. Because both photoluminescence and mechanoluminescence shows exactly the same wavelength emitted. Since photoluminescence is due to the Eu^{2+} than also the ML effect is due to that doping material. Moreover, comparing the spectra of the $\text{MoAl}_2\text{O}_4:\text{Eu},\text{Dy}$ and $\text{SrAl}_2\text{O}_4:(\text{Eu},\text{Dy})$, again it is possible see that the two peaks are in the same position and so it is an additional proof of Chandra theory.

References

- [1] Soon, S., & Jeong, M. (2014). As featured in Energy & Environmental Science. *Energy & Environmental Science*, 7, 3338–3346.
- [2] <http://www.dowcorning.com/applications/search/products/Details.aspx?prod=01064291>
- [3] Krishnan, S. (2015). Mechanoluminescent and Phosphorescent Paint Systems for Automotive and Naval Applications.
- [4] Ummartyotin, S., Bunnak, N., Juntaro, J., Sain, M., & Manuspiya, H. (2012). Synthesis and luminescence properties of ZnS and metal (Mn , Cu) -doped-ZnS ceramic powder. *Solid State Sciences*, 14(3), 299–304. Wang, J., Yan, C., Chee, K. J., & Lee, P. S. (2015).
- [4] Fontenot, R. S., Allison, S. W., Lynch, K. J., Hollerman, W. A., & Sabri, F. (2016). Mechanical, spectral, and luminescence properties of ZnS:Mn doped PDMS. *Journal of Luminescence*, 170, 194–199.
- [5] Jeong, S. M., Song, S., & Kim, H. (2016). Simultaneous dual-channel blue/green emission from electro-mechanically powered elastomeric zinc sulphide composite. *Nano Energy*, 21, 154–161.
- [6] Moon Jeong, S., Song, S., Lee, S. K., & Choi, B. (2013). Mechanically driven light-generator with high durability. *Applied Physics Letters*, 102(5). Peng, W. Q., Cong, G. W., Qu, S. C., & Wang, Z. G. (2006). Synthesis and photoluminescence of ZnS:Cu nanoparticles. *Optical Materials*, 29(2-3), 313–317.
- [7] Highly stretchable and self-deformable alternating current electroluminescent devices. *Advanced Materials*, 27(18), 2876–2882.
- [8] Wang, W., Huang, F., Xia, Y., & Wang, A. (2008). Photophysical and photoluminescence properties of co-activated ZnS:Cu,Mn phosphors. *Journal of Luminescence*, 128(4), 610–614.
- [9] Chen, L., Wong, M. C., Bai, G., Jie, W., & Hao, J. (2015). White and green light emissions of flexible polymer composites under electric field and multiple strains. *Nano Energy*, 14, 372–381.

- [10] Jha, P. & Chandra, B. P. (2013). Impulsive excitation of mechanoluminescence in SrAl₂O₄: Eu³⁺, Dy³⁺ phosphors prepared by solid state reaction technique in reduction atmosphere. *Journal of Luminescence*, 143, 280–287.
- [11] Laura English. A study of the synthesis and properties of zinc sulfide, *Private Communication*, 2016.
- [12] Luca Seghizzi, Jamie Blanchie, Dr. David Flynn, Dr. Helen Lewis, Prof. David Bucknall, Prof. Vicki Stone, Prof. Rebecca Cheung. Enabling Accurate Condition Monitoring with Embedded Nanoparticle Sensing. *Conference paper submitted to MFPT*, 2016.

3. Simulation of the behaviour of inorganic ZnS phosphors in the PDMS matrix

The aim of the simulation is a proof of concept study on how the stress is transferred from the matrix to the inorganic powder particles as a function of the volume fraction of the fillers.

As seen in the experimental tests, volume fraction plays a significant role in the threshold at which the elastico-mechanoluminescence (EML) appears and in the intensity of the emitted light. At low volume fractions of particles, a higher stress is needed to generate ML phenomena, and conversely at volume fractions above a critical value, the opposite is true. For practical applications, the condition we want to obtain in most of the cases is to have the lowest possible threshold to observe EML at low stress values.

In the paper [1] an analysis of ZnS doped powders of the GG series with the mechanical shaker were performed and light was detected. The density of powders used to make the sample was 7:3 ratio. Moreover, when these same GG phosphors were embedded in a PDMS matrix, EML was observed when the composite was oscillated in a stream of gas.²

Finite element analysis (FEA) using COMSOL Multiphysics and Abaqus 6.14 student version was performed to simulate the inclusion of inorganic mechanoluminescent particles in a polymer matrix. Results show that as predicted by Jha and Chandra³ there is a threshold stress value required to obtain EML for any particular volume fraction of ML particles. This critical stress value and volume fraction vary depending on the modulus of the matrix. When under an applied load, the resulting deformation causes direct contact between particles, which increases the stress inside the particles compared those not in close contact. This relative increase in stress changes the band structure of the ML materials due to a piezoelectric effect allowing an increase in electron transfer to the excited energy levels, which then relax back to lower energy states through luminescence. The net result is that

increases in stress applied to the ML composite material cause an increase in the ML intensity observed.

3.1. Material Properties

3.1.1. PDMS property

The PDMS is considered as an hyperelastic material that follows Odgen's model⁴ which is an analytical complex model used to describe the non-linear stress-strain behaviour of polymers and rubbers. It comes as an interpolation of experimental stress data obtained when PDMS is subjected to deformation. The interpolant equation depends on four constants that are given in the Table 3.1 and change depending on the percentage of curing agent used during the crosslinking process. Since in the Sylgard 184, the ratio 10:1 of PDMS : crosslinker seems to be used to have a good level of crosslinking, we have considered the following values for the model [4].

μ_1 (MPa)	0.244
μ_2 (MPa)	0.0146
α_1	1.018
α_2	3.74

Table 3.1. Ogden model constants for PDMS [4]

3.1.2. ZnS property

Modelling of ZnS is made considering its stress strain behaviour as anisotropic so that its compliance values are different for the three orthogonal axes. In the ideal models the ZnS particles are considered to be spherical. Later FEA analysis has been applied to real, “non-ideal”, systems. The compliance values are taken from [5] and adapted for the Abaqus matrix. What we obtain is a matrix 6X6 giving the values seen in the matrix below:

$$\begin{vmatrix} D_{11} & D_{12} & D_{13} & D_{14} & D_{15} & D_{16} \\ D_{21} & D_{22} & D_{23} & D_{24} & D_{25} & D_{26} \\ D_{31} & D_{32} & D_{33} & D_{34} & D_{35} & D_{36} \\ D_{41} & D_{42} & D_{43} & D_{44} & D_{45} & D_{46} \\ D_{51} & D_{52} & D_{53} & D_{54} & D_{55} & D_{56} \\ D_{61} & D_{62} & D_{63} & D_{64} & D_{65} & D_{66} \end{vmatrix} = \begin{vmatrix} 209.7 & 121.1 & 105.1 & 0 & 0 & 0 \\ 0 & 209.7 & 105.1 & 0 & 0 & 0 \\ 0 & 0 & 210.9 & 0 & 0 & 0 \\ 0 & 0 & 0 & 42.5 & 0 & 0 \\ 0 & 0 & 0 & 0 & 42.5 & 0 \\ 0 & 0 & 0 & 0 & 0 & 44.3 \end{vmatrix}$$

Equation 3.1. Compliance values of ZnS crystals

From the matrix (Equation 3.1), it can be seen that the most significant deformation occurs along the three major axes, i.e. the D_{11} , D_{22} , D_{33} axes. However, in the experiments using powdered phosphors, they are polycrystalline and therefore modelling their orientation relative to any specified direction is unrealistic. However, an analysis was made to compare the materials in isotropic and non-isotropic situation. A strain of 10% was applied to an isotropic spherical particle and an identically sized non-isotropic particle with the stress along the D_{11} axis, i.e. along the axis where the compliance is the largest.

The resulting stress values showed that particles deformed in a very similar way, a difference in the maximum stress value of 0.06 MPa was found.

Consequently, the simpler isotropic model was used in all subsequent computational model simulations and an average elastic modulus value was considered. This simplification

represents a simpler situation in which it is possible to think that the anisotropic behaviour is lost in the sample since the impossibility to orient all the particles along a determined axis. Therefore, as an average, an isotropic behaviour is a better generalization of the phenomena. The ZnS particles were then model assuming a modulus of 98.1 GPa, Poisson's ratio of 0.41, and density for ZnS equal to 4.09 g/cm³ was used. [6]

3.2. Modelling procedure

The FEA modelling was undertaken considering three different configurations and the complexity of the model was increased with the different steps.

- 1- To understand ZnS-PDMS interactions the initial model considered a single ZnS particle in a PDMS matrix. The easiest way to study this first case is to model a single particle in a PDMS matrix. In this way it is implied that every ZnS particle is isolated from the others and so no interactions are present. Moreover, the ZnS particle is considered a sphere or a circle to avoid issues of shape anisotropy.
- 2- Mechanoluminescent ZnS : PDMS systems reported in the literature [7-11] all exploit a 7:3 ration of weight of particles to PDMS. This means that the particles are in close contact and in some case they touch each other. Hence, modelling is needed to verify how the intensification of stresses influences the system behaviour.
- 3- Finally, a more realistic situation is needed to try to understand fully how the system behaves with shape anisotropy and irregular particle spacing.

Initial modelling utilized Abaqus software for the simplest models where imprecision in the results occurred because of the limited number of meshing elements available. However, in these simple models these issues did not invalidate the results. For the more complex models subsequent simulations were performed using Comsol Multiphysics 5.0 where more precision in the results was required.

3.2.1. Single particle model

3.2.1.1. 2D Geometry

In this initial FEA analysis using Abaqus software, the 2D model consisted of a PDMS matrix as a rectangle of $(200 \times 60) \mu\text{m}$ containing a circular particle of radius of $20 \mu\text{m}$. The dimensions of the ZnS were chosen based on particle sizes observed by SEM [1]. In this ideal system the circular particle geometry was placed in the centre of the matrix rectangle. Once the initial geometry was established in the Abaqus software, the mechanical properties given in Section 3.1.1 and 3.1.2 were attributed to the two materials.

A mesh was generated and applied to the geometry and the circular partition. Abaqus mesh permits the choice of the correct mesh level with a different precision depending on the specific geometry. The software allocates the various mesh elements following a linear or a quadratic simulation, the difference between the two situations is in the number of nodes that are taken into consideration. In the first case, 4 nodes are considered whilst in the second case 8 nodes are chosen to increase the precision. For the elastomer rectangle a linear mesh was adopted, because it requires the least precision, whilst for the circular ZnS particle, a quadratic mesh was used to increase the simulation precision. At the interface between the particle and the matrix, the mesh precision was increased for the transition

from the linear to quadratic meshes providing better precision in the region which is very important for this study.

To replicate the forced oscillation experiments performed in the laboratory, the simulation also holds one of the shortest sides of the rectangular sample geometry in a fixed position in space whilst the strain is applied to opposing side of the sample. In the subsequent images the sample is held on the right-hand edge and the stress is applied horizontally to the left-hand edge.

The interaction between the particle and the matrix was varied to establish its significance in the stress transfer within the composite. The exact nature of the bonding between the PDMS matrix and ZnS in real systems has not been determined, so two ideal situations were applied to perform the simulations. In one case, the PDMS is assumed to be completely bonded with the ZnS particles, and this was compared to the second situation where there was assumed to be no interaction between the PDMS and the ZnS particle. Whilst these are extreme cases nevertheless these situations were explored to provide insights into the influence of the interface interaction strength on stress transfer in the system.

Full bonding between the PDMS and ZnS within the Abaqus software, was represented by allowing tie contacts between matrix and particle. The results of the simulation under an applied stress strain of 10% of the dimension of the sample that increase in the time of one second can be seen from the contour plot of the von Mises stress shown in Figure 3.3. As the contour plot shows there is significant stress that is transferred from the matrix across the interface boundary into the ZnS particle.

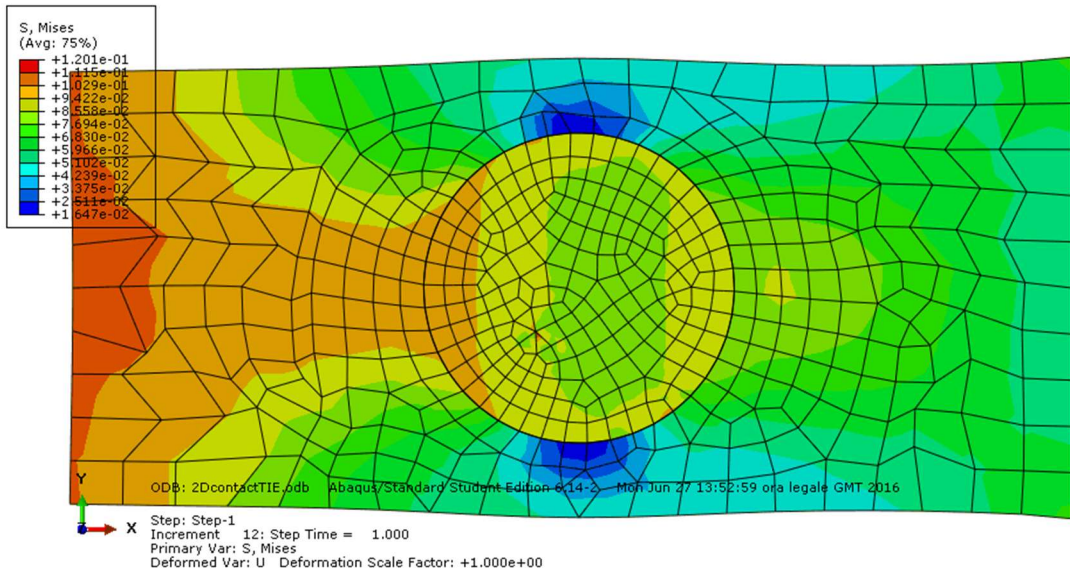


Figure 3.1. Circular ZnS particle embedded in a rectangular PDMS region. The stress is applied along the X axes and toward left while it was fully constrained on the left hand side. In this case a full stress transfer between PDMS and ZnS with indication of different magnitude of Von Mises stresses.

The PDMS is constrained on the right hand side while pulled with a force normal to the edge on the left hand side.

Moreover, analysis of the average stress within the ZnS particle as a function of strain (see Figure 3.2) shows a linear increase of stress with increasing strain applied to the matrix. This linear behaviour is consistent with expectations for elastic materials that follow the well-known relationship, $\sigma = E \cdot \epsilon$ where σ is the stress, ϵ the strain and E is the Young modulus.

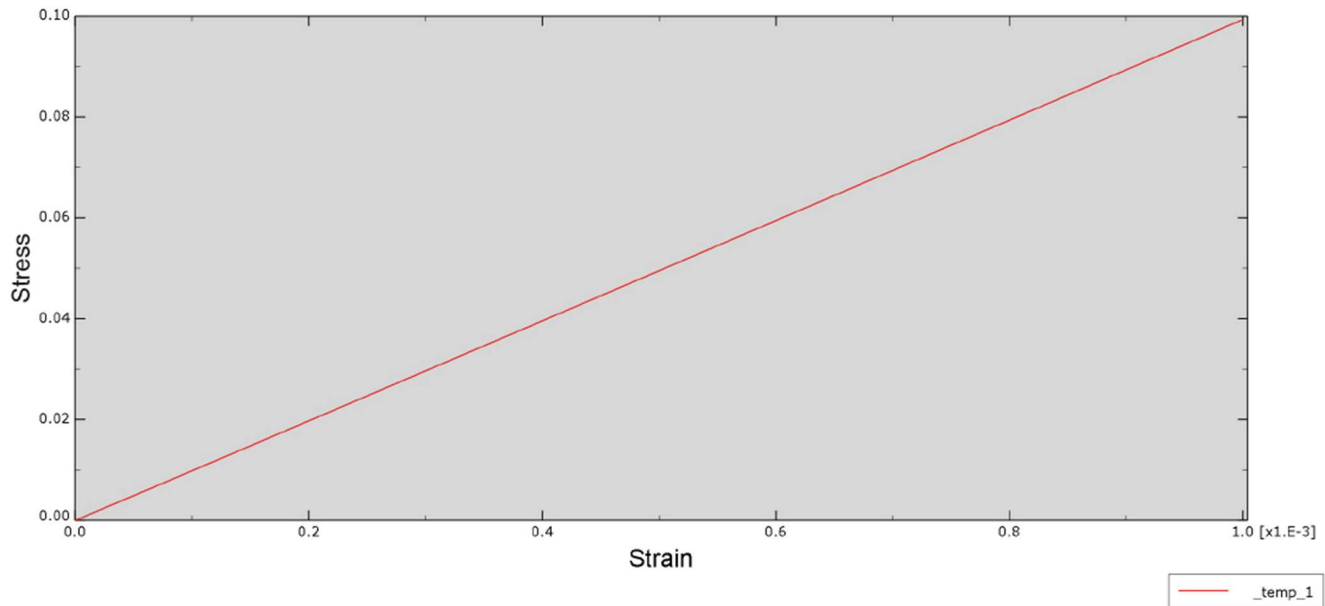


Figure 3.2. Stress-strain behaviour of ZnS elastic material in the full stress transfer between PDMS matrix and inorganic particle.

From the graph it is possible to evaluate that the maximum stress value is 0.1 MPa at a maximum strain of 10^{-3} .

The simulation was repeated, but in this case the interfacial bonding between the PDMS and the ZnS particle was set to zero. The results of the simulation (see Figure 3.3) are very different from the previous case, and shows that there is no stress transfer between the PDMS matrix and the particle. In this case there is no stress increase observed in the particle has a blue colour meaning that no stresses are present. The stress applied to the system is only seen in the matrix.

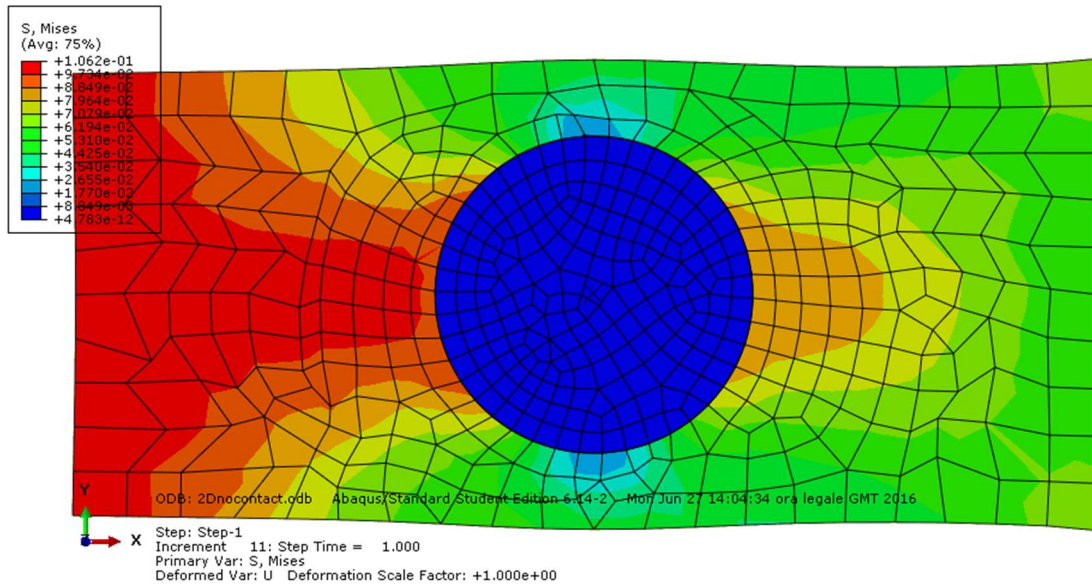


Figure 3.3. Circular ZnS particle embedded in a rectangular PDMS region. The stress is applied along the X axes and toward left while it was fully constrained on the left hand side. In this no contact between matrix and particle is present. Von Mises stresses are represented with the legend on the left hand side.

The distribution of stresses is different from the situation above and in the particle no stress is present.

As before, the stress and strain behaviour within the ZnS particle was evaluated, the results of which are shown in Figure 3.4. The results are plotted as a function of time since within error the stress and strain experienced by the ZnS particle is effectively zero.

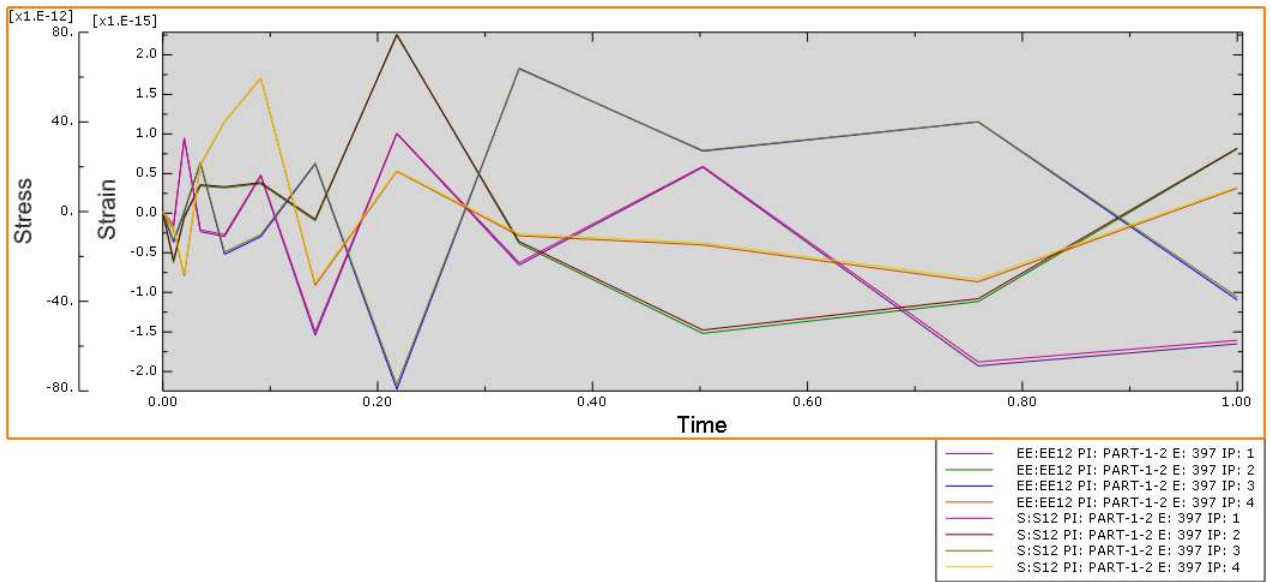


Figure 3.4. Stress and strain function of time. There should be a line at values of zero, the model is imprecise.

A more precise model is obtained with the 3D case where this imprecision will be cancelled as seen in the next chapter.

3.2.1.2. 3D Geometry

The 3D geometry is slightly more complicated as it has to be created. The particle was described by a sphere with a diameter of $20\mu\text{m}$, and the PMDS matrix was made with a spherical cavity in the middle. The dimensions of PDMS are $(200 \times 60 \times 40) \mu\text{m}$ while the sphere has a radius of $20\mu\text{m}$. To produce an accurate and uniform mesh for the sphere it was necessary to use the ‘face to datum on plane’ option, which enables division of the sphere in 8 equal zones so that a uniform mesh is obtained once applied.

The sphere is treated as a rigid body and in the initial simulations tie contacts with the PDMS are included, so that full stress transfer between matrix and particle occurs.

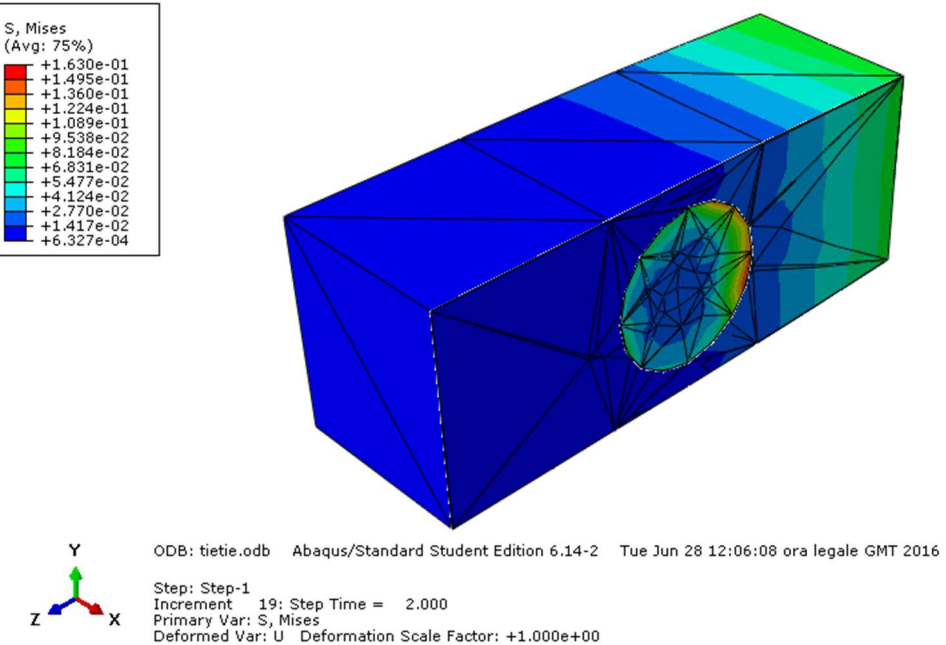


Figure 3.5. Cross-section through the 3D simulation geometry showing full stress transfer between the spherical ZnS particle in the PDMS matrix.

The result of a simulation at a strain of 10^{-3} is shown in Figure 3.5, which shows the values of the von Mises stress in the composite. In Figure 3.5, the composite is held fixed on the left hand vertical face and strain was applied to the opposing face, i.e. the right hand side in Figure 3.5. The magnitude of the von Mises stress are shown by the different colours as indicated by the legend on the top left hand side of the figure. It is possible to clearly see an intensification of stress in the right hand side of the particle.

Analysis of the average stress within the particle as a function of strain is shown in Figure 3.6. The linear elastic behaviour observed by the ZnS is the same as that obtained for the 2D model. I.e., no differences between the two Young moduli and their behaviour is present.

Plotting the stress VS strain graph, we can see that there is no difference between the 2D and the 3D model, because at value of strain of $0.7 \cdot 10^{-3}$, the value of the stress is around 0.06 MPa.

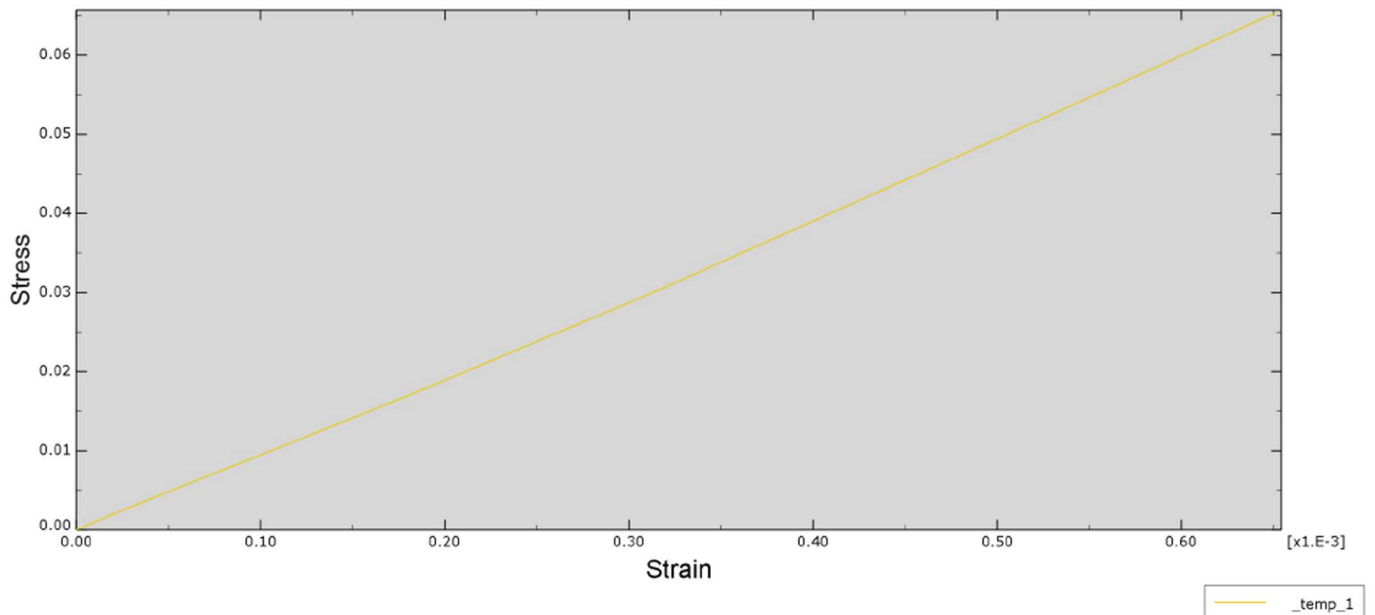


Figure 3.6. Stress versus strain plot of the ZnS inorganic particle.

When the simulations are repeated assuming no bonding between the ZnS and the PDMS, the resulting distribution of the von Mises stress within the composite can be seen in Figure 3.7. As can be seen, despite a strain of 7×10^{-4} applied to the composite resulting in maximum von Mises stresses of ~ 0.09 MPa in the PDMS, there is no stress observed in the ZnS particle. Analysis of the stress and strain as a function of the time strain is applied to the composite is shown in Figure 3.8. As expected with zero interaction between the PDMS and the ZnS, there is no stress (or strain) transferred from the PDMS to the particle. Additional detail is observed in this 3D model that was not seen in the 2D model, since it is possible to see a small degree of debonding between the particle and the matrix with void formation between the two.

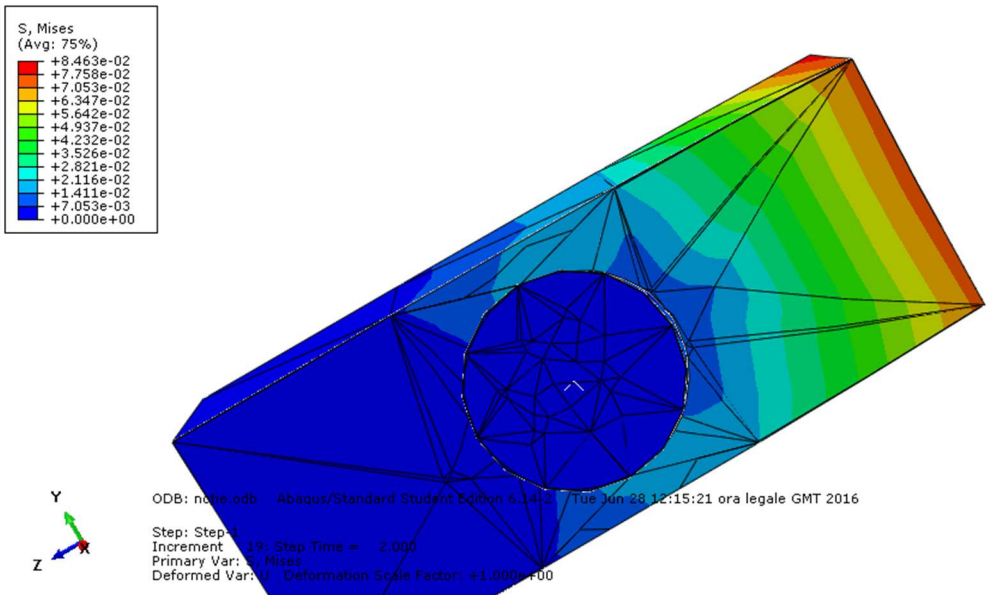


Figure 3.7. No stress transfer representation between matrix and particle with a void formation next to the right hand side of the particle

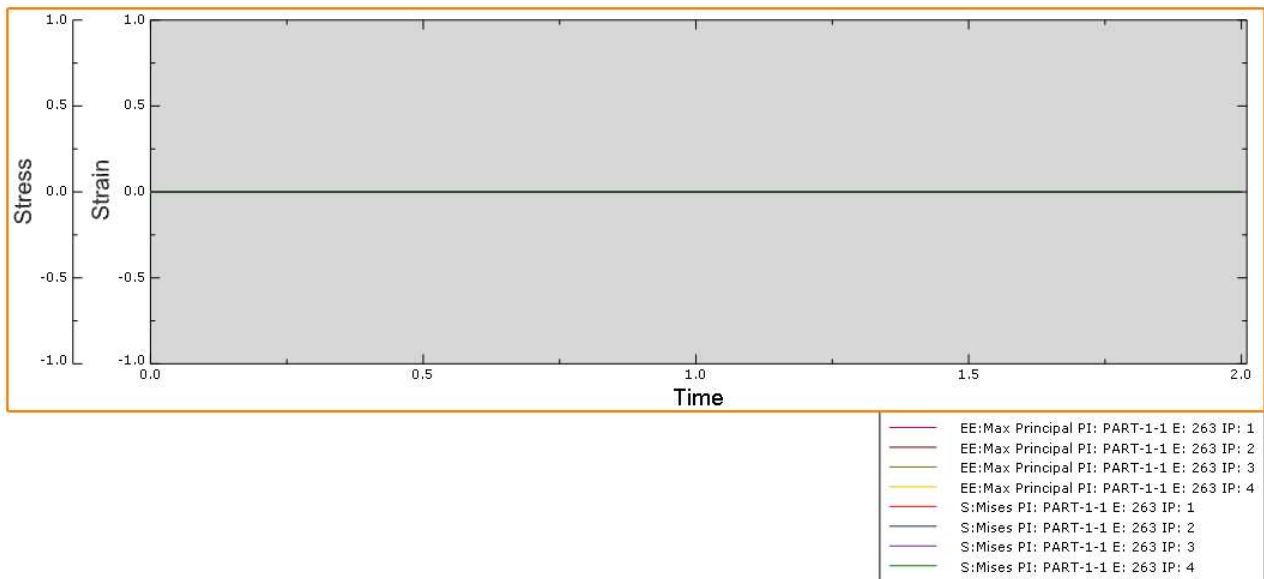


Figure 3.8. Stress and strain plot vs time. There is no stress transfer so the value of stress and strain is zero.

3.2.2. Two particles system geometry

In many experimental studies of ML from ZnS/PDMS composites [7-11], a ratio of 7:3 for ZnS and PDMS is always used. This mean there is a high volume fraction of the ML phosphors in the polymeric matrix. Therefore, there is the need to investigate how the stresses in the composite changes in the case in which two (or more) particles are in contact between each other.

What it is expected is indeed an increase of the stress at the contact point between two particles, because of the stress definition, $\sigma = F/A$ where F is the force applied and A is the area over which the force is applied. By inspection of this equation it is clear that stress increases as the area of contact decreases. From contact mechanics theory, it is known that two spheres in contact have a contact area, A , defined by the contact radius, r , which depends directly on the force applied. The contact radius is given by:

$$r = \sqrt[3]{\frac{3F \left(\frac{1 - \nu_1^2}{E_1} + \frac{1 - \nu_2^2}{E_2} \right)}{4 \left(\frac{1}{R_1} + \frac{1}{R_2} \right)}}$$

Equation 3.2. Contact radio between two spheres in contact. E is the Young modulus, ν is the Poisson's ratio and R is the radio of the two spheres.

where E_1 and E_2 , are the Young's modulus for two spheres 1 and 2, ν_1 and ν_2 are the Poisson's ratio of the two spheres, and R_1 and R_2 are the radii of the two spheres, respectively.

The modelling was undertaken by including two ZnS particles in a PDMS matrix as shown in Figure 3.9, which shows the results of applying a strain to the left hand edge of the composite and holding the right hand edge fixed. This as a proof of concept, shows as result that there is an intensification of stresses in the contact point between the two particles as shown in figure 3.11.

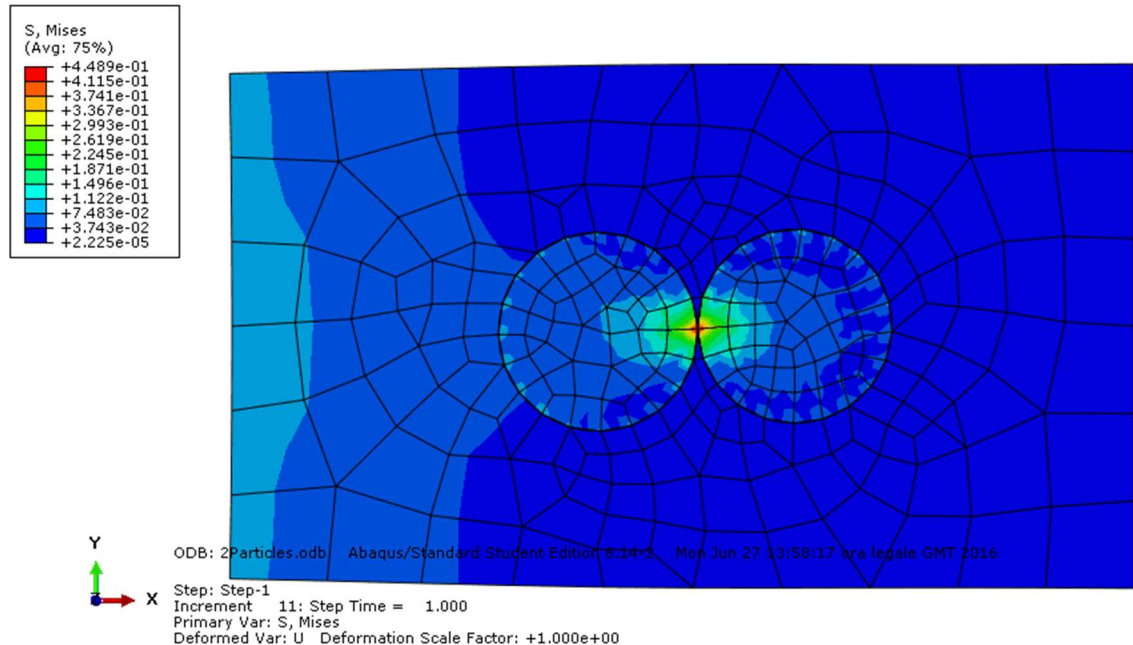


Figure 3.9. Two particles with a tangent contact and full stress transfer between particles and matrix. It is clear the intensification of stresses in the contact point.

The von Mises stress have different values in the matrix and in between the two particles, with a stress intensification observed at the contact point of the two particles. The value of the stress in this region are five times higher than seen in the case of a single ZnS particle in PDMS that experiences the same strain.

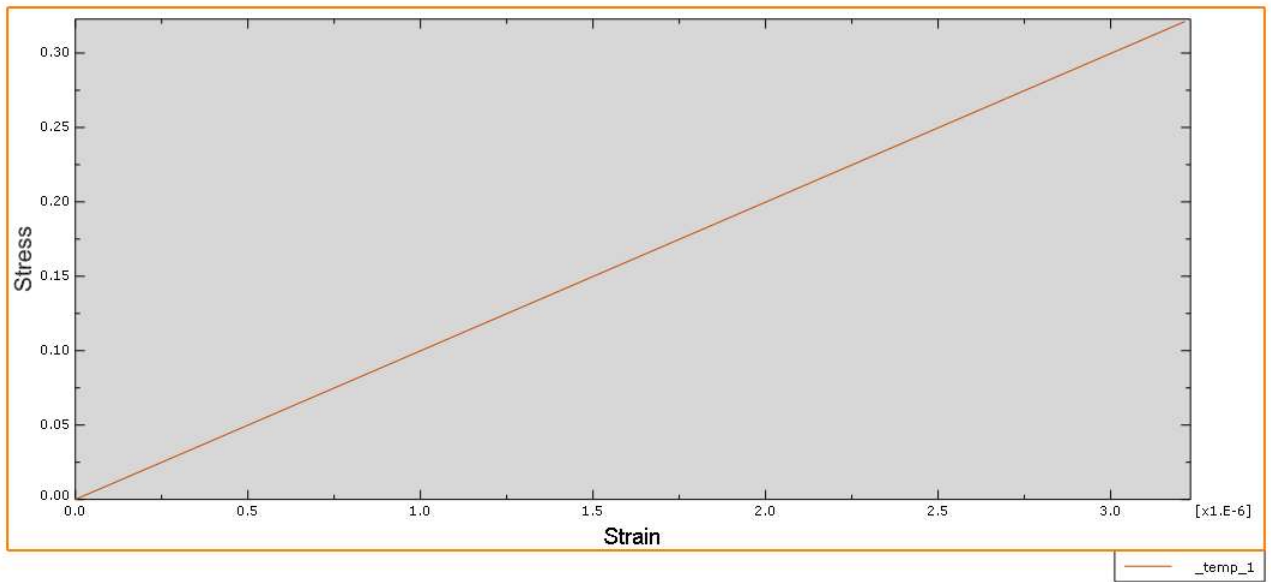


Figure 3.10. Stress vs strain of two particles in contact. The maximum stress is higher than in the case of single particle in PDMS matrix.

Analysis of stress in the region of the contact area of the two particles as a function of strain is shown in Figure 3.10. The apparent discrepancy in maximum stress observed in Figures 3.9 and 3.10 is due to the limits of the mesh used in these simulations. Having rectangular mesh elements that are too big produces a large degree of inaccuracy around the contact point. So, the exact position of the contact point can't be selected precisely to analyse the stress-strain behaviour.

3.3. Complete system modelling

The simulations described in the previous sections were deliberately undertaken as they are relatively easy to set up and compute, whilst providing useful feedback for the more complex simulations. The preceding models are all idealised and incorporated circular or spherical ZnS, in PDMS matrices with no other particles in the matrices. Given the high volume fraction of particles in experimental composites, more realistic models are needed.

Therefore, a much better way to try to reproduce the real case is to start from a picture of a real sample and utilize this to extract the start geometry for the FEA modelling.

A scanning electron microscopy (SEM) image of a ZnS : PDMS composite at a 7:3 ratio [1] is shown in Figure 3.11. By the very nature of SEM imaging, which has a very large depth of field, the image is effectively 3-dimensional. Therefore, in order to use this for FEA modelling it is necessary to extract a 2D equivalent model geometry from the 3D image. The extracted geometry can then be imported into Abaqus or Comsol. The process described below is general and can be applied to any 3D image.

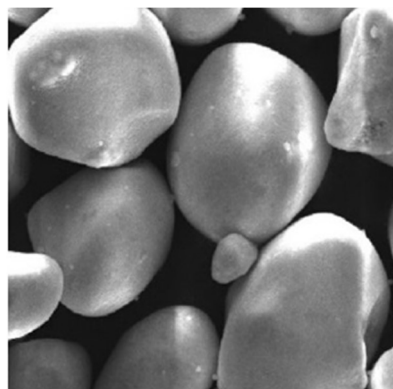


Figure 3.11. SEM image of a ZnS:PDMS composite taken from reference [1]

Although dedicated image analysis software is available for some of the processing described below, these were not available for this project. None of the available image analysis software is designed to translate images to mesh structures required for FEA simulations. Therefore, an important part of the processing was to develop codes to incorporate all the elements necessary to allow meshing geometries able to be input directly into Abaqus or COMSOL in order to perform the analysis.

Moreover, there are more precise software that permits to create a 3D image directly from the sample itself and to import it in Abaqus. An example is the Materialise Mimics software that allows to convert images from MRI (magnetic resonance imaging) directly into Abaqus in 3D.

The first step used in the mesh model creation was to apply a basic increase of the image contrast and brightness, thereby deleting the shadows to give a corrected image shown in Figure 3.12. Although not essential this step helps to obtain a clearer final image. This step was undertaken using Photoshop express (running on a Windows 10 operating system).



Figure 3.12. Manually modification of the image increasing contrast and brightness and deleting shadows.

3.3.1. Image segmentation

Pixelation of the images results in a blurring of the image at the edges between black and white regions with a grey scale gradient forming a blurred boundary between them. It was therefore necessary to modify the image to sharpen the boundaries between black and white regions. This process is called image segmentation and is a technique of imaging processing usually used in computational biology [12] or in biometric i.e. for fingerprint segmentation [13].

To perform this operation, a short code was written in Python and implemented on Figure 3.12. Python is an object programming language that requires libraries containing appropriate functions and tools needed for the processing, these are called as follows:

```
import numpy as np
from PIL import Image
from matplotlib import pyplot as plt, cm
from skimage import io
from skimage import img_as_float
```

The desired image file can then be opened and imported and converted into an array using the following code:

```
x=Image.open("C:\\\\Users\\\\luca\\\\Desktop\\\\image.png", 'r')
x=x.convert('L')
y=np.asarray(x.getdata(), dtype=np.float64).reshape( (x.size[1],x.size[0]))
y=np.asarray(y, dtype=np.uint8)
w=Image.fromarray(y, mode='L')
w.save("C:\\\\Users\\\\luca\\\\Desktop\\\\fotogray.png")
```

The result is the grayscale image shown in Figure 3.13. This image can now be manipulated:

```
im = io.imread("C:\\\\Users\\\\luca\\\\Desktop\\\\fotogramy.png")
plt.imshow(im, cmap='gray')
plt.show()
```



Figure 3.13. Greyscale image

It is important to understand how the pixels are distributed and which grey scale level they have. A histogram function is used in order to visual the grey level separation:

```
from skimage import exposure
histogram = exposure.histogram(im)
plt.plot(histogram[1],histogram[0])
plt.show()
```

The resulting histogram from this analysis is shown in Figure 3.16.

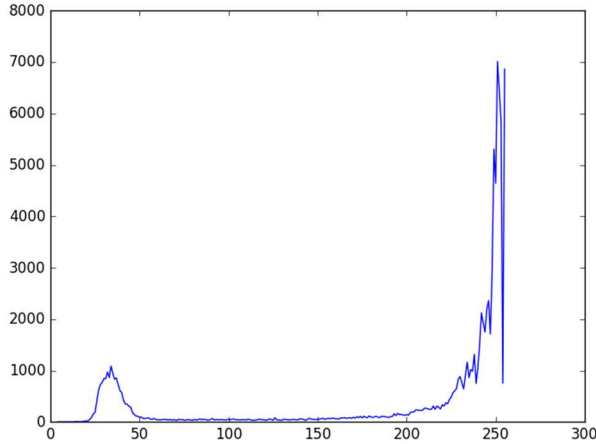


Figure 3.14. Histogram of the grayscale of the modified image. On the Y axes, the relative intensity of the colours is present. On the X axes there is the distribution of colours, with two peaks in the left and right hand side and no intensity in the middle. The left and right represent the black and white pixels while in the middle, all the shades of grey are shown.

The histogram shows that the values are well distributed, so there is no overlap between black and white region in the middle. To make a comparison, taking for example the initial image (Figure 3.11) and with applying any image correction, the resulting histogram is shown in Figure 3.17.

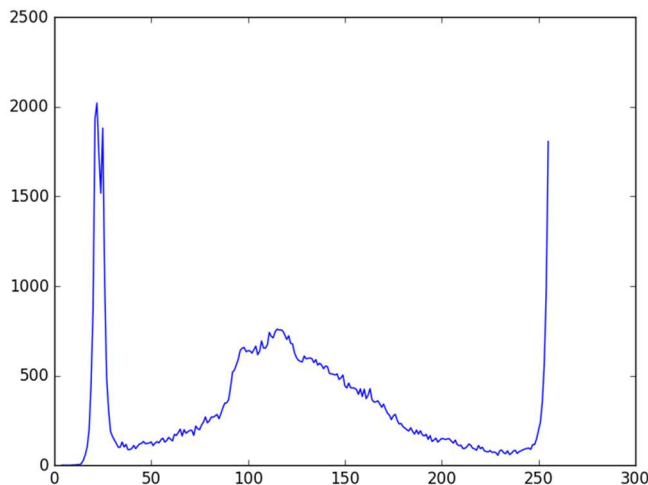


Figure 3.15. Histogram of the grey scale of the unmodified image. On the Y axes, the relative intensity of the colours is present. On the X axes there is the distribution of colours, with two peaks in the left and right hand side and no intensity in the middle. The left and right represent the black and white pixels while in the middle, all the shades of grey are shown.

This means that there is less separation of colours. In the centre of the plot a broad peak is seen that gives all the grey tonality to the image. Clearly the best image processing results are obtained with the colour separation seen in Figure 3.14.

The next step is to create a threshold value that will separate the grey values from the background with the ones of the image we want to obtain i.e. the difference of grey between particles and the PDMS matrix in background.

It is possible to do it manually, but there is a dedicated function for this process in Python which was implemented. This function automatically computes the best threshold and is present in the Numpy's Python library where also the filters that are need in later steps can be found.

```
from skimage import filters
threshold = filters.threshold_otsu(im)
print(threshold)
fig, ax = plt.subplots(ncols=2, figsize=(12,8))
ax[0].imshow(im, cmap='gray')
ax[0].contour(im, [threshold])
ax[1].imshow(im < threshold, cmap='gray')
plt.show()
```

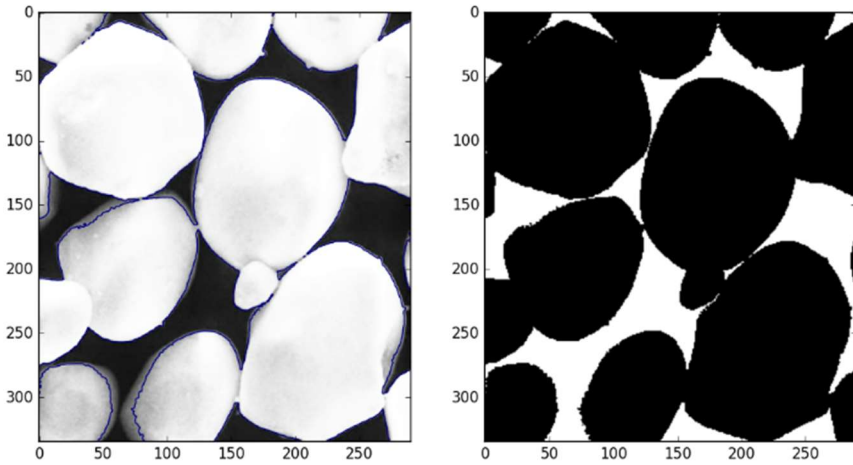


Figure 3.16. On the left hand side, it is possible to see the threshold border on the starting image and on the right hand side the binary image resulting after the segmentation.

The results of adding the threshold values is shown in the left hand side of Figure 3.16, where it is possible to see the threshold border as a blue line that marks the separation between the white and black regions. Once the threshold value has been assigned it is straightforward to binarize the image as shown on the right hand side of Figure 3.16. The binary image shows a sharp separation between the black and white regions. The black regions represent the ZnS particles and the white regions the PDMS matrix.

Careful examination of the binary image (see Figure 3.17) shows that the blue threshold line is not exactly in the correct place, so the image is not very precise. More importantly, it is possible to see that the edges of the regions are not smooth. Therefore, the next step eliminates these defects by making the edges as smooth as possible to avoid additional work later when the final image will be imported in the Comsol software.



Figure 3.17. Zoom on the edges of particles, they are not smooth and lot of imperfections can be seen.

To achieve this a filtering process is needed to remove the noise in the pre-binarized threshold image (left hand side of Figure 3.16) to form a sharper separation between the various pixels and increase the precision of the thresholding function. It is therefore necessary to group pixels that are close together and assign them to the same face, i.e. to the particle. To do so a function called a median filter was utilised, which allows every pixel to be taken by its surrounding, and then the median value of that area is computed to give a single value.

Obviously the more pixels that are chosen in a window, the less precise the average values will be due to increased standard deviation. To avoid this issue, a common procedure is to select window sizes that matches the radius of curvature appropriate to the shapes used in the image. The following code implements this:

```
from skimage import restoration
median_filtered = filters.median(im, np.ones((7,7)))
plt.imshow(median_filtered, cmap='gray')
plt.imshow(median_filtered [390:410,820:840],cmap = 'gray', interpolation
='nearest')
plt.colorbar()
print (median_filtered [390:410,820:840].std())
plt.imshow(median_filtered,cmap= 'gray')
plt.show()
```

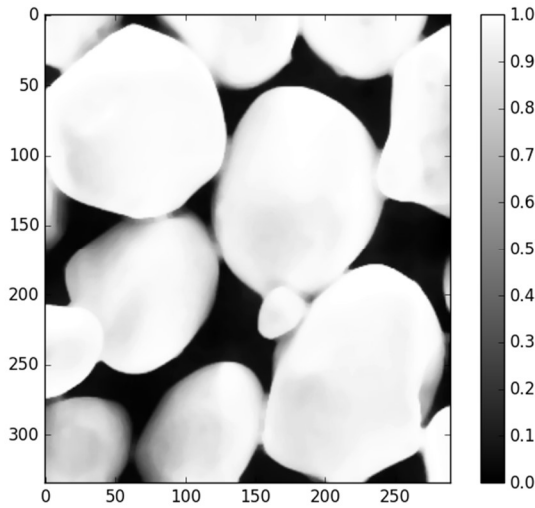


Figure 3.18. Image obtained after the filtering process

The application of this filtering to the Figure 3.13 is shown in Figure 3.18. Although the image appears blurred to our eyes, there is a much better division of pixels, from which it is possible to obtain a binary image as desired and with almost no defects. Apply binarization code:

```
binary_image = median_filtered <filters.threshold_otsu(median_filtered)
plt.imshow(binary_image,cmap='gray')
plt.show()
```

results in the binary image shown in Figure 3.19. Some edges of the black regions are still not perfectly smooth, which could be improved simply reducing the windows size further. However, for the purposes of this thesis, Figure 3.19 is good enough to work with.

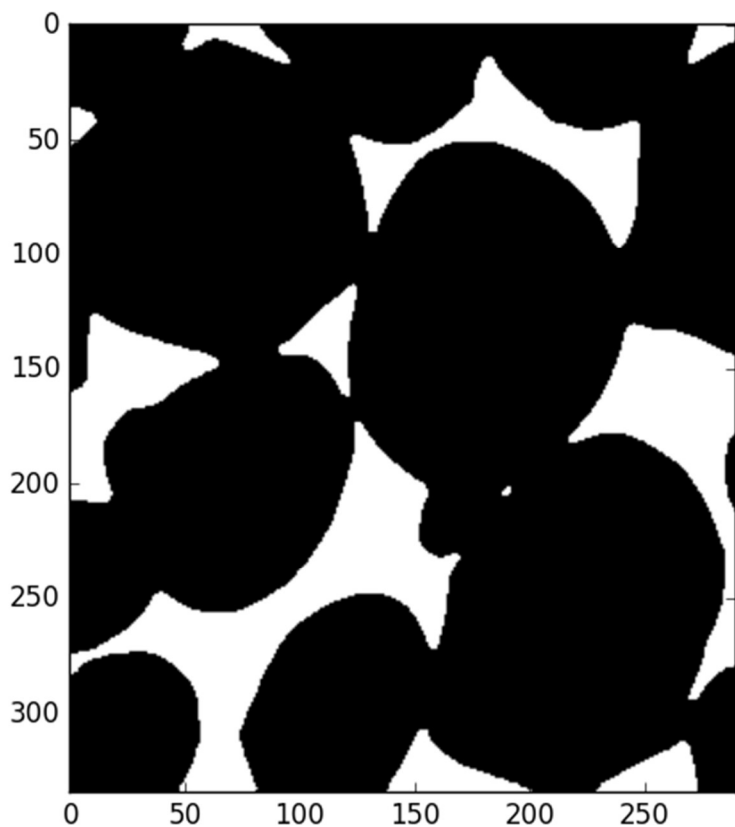


Figure 3.19. Final binary image obtained after the filtering process

3.4. Mesh Generation from the binary image

The following step generates a mesh from the binary image and exporting the mesh to the COMSOL software in order to perform the finite element analysis.

Initially the binary image was imported into Matlab, and using its own built in functions, the boundary between the two regions were identified:

```

I = imread('C:\Users\luca\Desktop\imagefrompython.png');
BW = I < 100;
imshow(BW);
[B,L] = bwboundaries(BW);

```

The boundary function extracts the coordinates of the edges. Subsequently it is necessary to manually extract every boundary obtained in this way and group them together. These will constitute the nodes of the final image.

Nodes are defined as XY coordinates of the geometry vertices and the vertices for all face have to be specified before the meshing is implemented and can be specified in any order. This is very important because, the program starts from one node and creates the mesh of all the others nodes without any discontinuities. This means that there can be the situations where two nodes are at extremities of the image between which a line will be connected, passing across the whole image ruining the final result. Therefore, the fact that the position of the nodes is arbitrary, it is possible to obtain a sequence of all the nodes such that no connection line pass through any other shape, but it connects a little portion of space just enough to connect two close nodes.

Because the phases are kept as independent shapes, they need to be connected with a unique final mesh. The Matlab code to achieve this is:

```

node1= B{1,1} (:,1:2);
node2= B{2,1} (:,1:2);
node3= B{3,1} (:,1:2);
node4= B{4,1} (:,1:2);
node5= B{5,1} (:,1:2);
node = [node1;node2;node3;node4;node5];

```

A couple of further operations are needed to create the edges of the boundaries that will be used when implementing the Mesh2D meshing package:

```
n1 = size(node1,1);
n2 = size(node2,1);
n3 = size(node3,1);
n4 = size(node4,1);
n5 = size(node5,1);
e1= [(1:n1-1)', (2:n1)'; n1,1];
e2= [(1:n2-1)', (2:n2)'; n2,1];
e3= [(1:n3-1)', (2:n3)'; n3,1];
e4= [(1:n4-1)', (2:n4)'; n4,1];
e5= [(1:n5-1)', (2:n5)'; n5,1];
edge = [e1;e2;e3;e4;e5];
```

The Mesh2D sub-routine is simply applied using:

```
[P,t] = mesh2d(node,edge);
```

The resulting mesh can be seen in Figure 3.20. It is possible to see that there is a different mesh size in different regions of the image, next to the edges it is denser than in the middle.

Moreover, in the bottom left region of the image, a mistake is seen, introduced by the node continuity that links two parts of the image. Ultimately this is not a problem because when imported into COMSOL, it is possible to remove all that imperfections.

Finally, as indicated above, although this is not a faithful replication of the original image of the real system, this *modus operandi* works for every situation, so, taking a 2D image there will be the mesh for the real and more precise model.

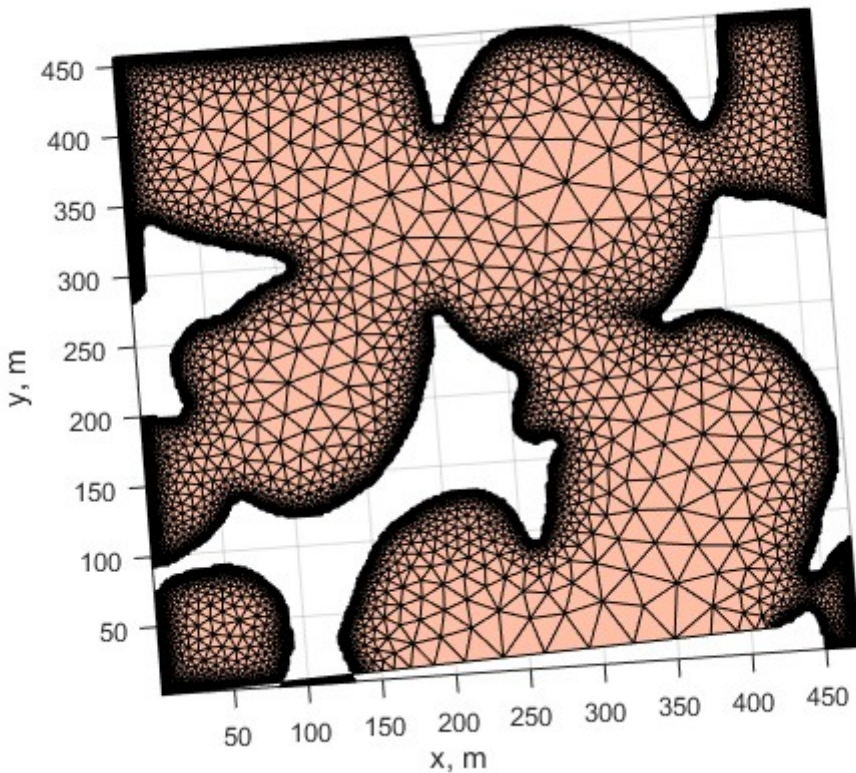


Figure 3.20. Mesh generated with Mesh2D from the binary image

3.4.1. Importing the .mat file in Abaqus

Ideally the *.mat* file containing the mesh could be imported directly into Abaqus as an *.inp* file. Unfortunately, Matlab export files are encrypted, so saving the mesh simply as *.inp* file will not work.

Hence, to perform the operation, it is necessary to understand what it was created with the Matlab mesh command and how an *.inp* file work.

Mesh2D creates an array of XY coordinates, as well as an array of triangles. These coordinates can be saved as a *.txt* file. This *.txt* file can further be modified to reproduce the

exact language with the logic point used by Abaqus. Moreover, there are two sets of coordinates, one is for the nodes and the other are the elements that are needed to be defined with Abaqus labels.

In addition, a line needs to be added in before every set of coordinates for both the elements and the nodes. This line is just an ordinate and growing series of numbers, that is needed to be used. Indeed, Abaqus does not recognise the set point as coordinate if each of them is not numbered.

Once these operations have been performed, the mesh *.inp* file can be imported into Abaqus.

3.4.2. Importing mesh into Comsol

Like Abaqus, COMSOL can not read the *.mat* files directly. Hence, to convert into the required Nastran file it is necessary to vectorise the matrix, giving an orientation to all the faces (since the following is in 2D, there is only one face).

To do this operation it is necessary perform triangulation of the matrix and then compute the normal to that. It is an easy operation with two Matlab function:

```
TR = triangulation(P,t);  
normals = vertexNormal(TR);
```

In order to be able to implement the *Matnastran* Matlab package which works for 3D meshes, it is necessary to pad the data array with add a line of zeros to the 2D image data and then extract the normal:

```
P(1,3:3)=0;
```

```
normals(size(t),1)=0;  
normals(:,3:3)=1;
```

Matnastran can finally be run to obtain the desired *.nastran* file that can be imported into COMSOL.

```
run('matnastran');
```

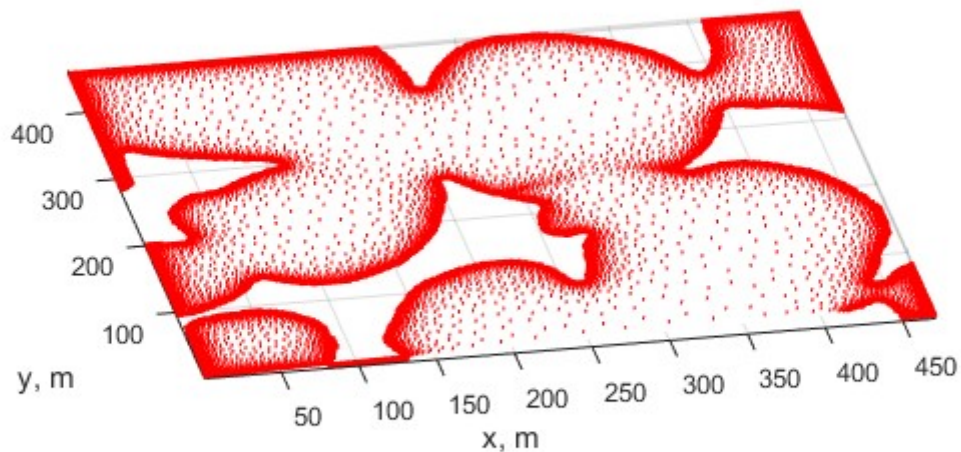


Figure 3.21. Matlab vectorised mesh. The red dots are arrows pointing up. Each arrow is in a node of the triangulation.

The results of this mesh and vector normal calculation is shown in Figure 3.21, where it is possible to see that all the red dots are in fact arrows that represent the vectors of the image at each mesh node point.

3.5. COMSOL

Comsol Multiphysics is a powerful program suite that allows finite element analysis, solver and simulation software for various physics and engineering applications, especially for coupled phenomena.

COMSOL contains a very powerful tool that allows any mesh to be imported and then transform them to any geometry very easily, and for this reason for the current purposes it was preferred over Abaqus. Once the mesh is imported, it is then necessary to complete the operation by simply drawing a rectangle around the geometry that represent the PDMS matrix. There are therefore two different zones, the particles and the matrix drown.

It is now possible to manually segment the image, deleting extra parts as required, dividing the particles and clean the edges of the particles itself.

This operation is fundamental because there will be some edges that otherwise have a few imperfections, which requires manual deletion of some nodes. This operation is linked to the precision of the window of the reshaped image discussed in Section 3.3.1. The more the model is precise, the less operations are needed at this stage. In other words, the greater the edge smoothness, the fewer operations are required.

COMSOL has a huge library of materials, which include data for find both the PDMS and the ZnS. The property values of these materials were modified to match those used for the Abaqus simulations described above.

Within COMSOL, the known physics and boundary conditions must be added, which match the same conditions used in Abaqus, that define the stress input. In the following results, the right hand side of the sample is held at constant load applied normal to the edge on the left hand side

The von Mises stress map of the realistic ZnS distribution at a strain of 0.1 is shown in Figure 3.22.

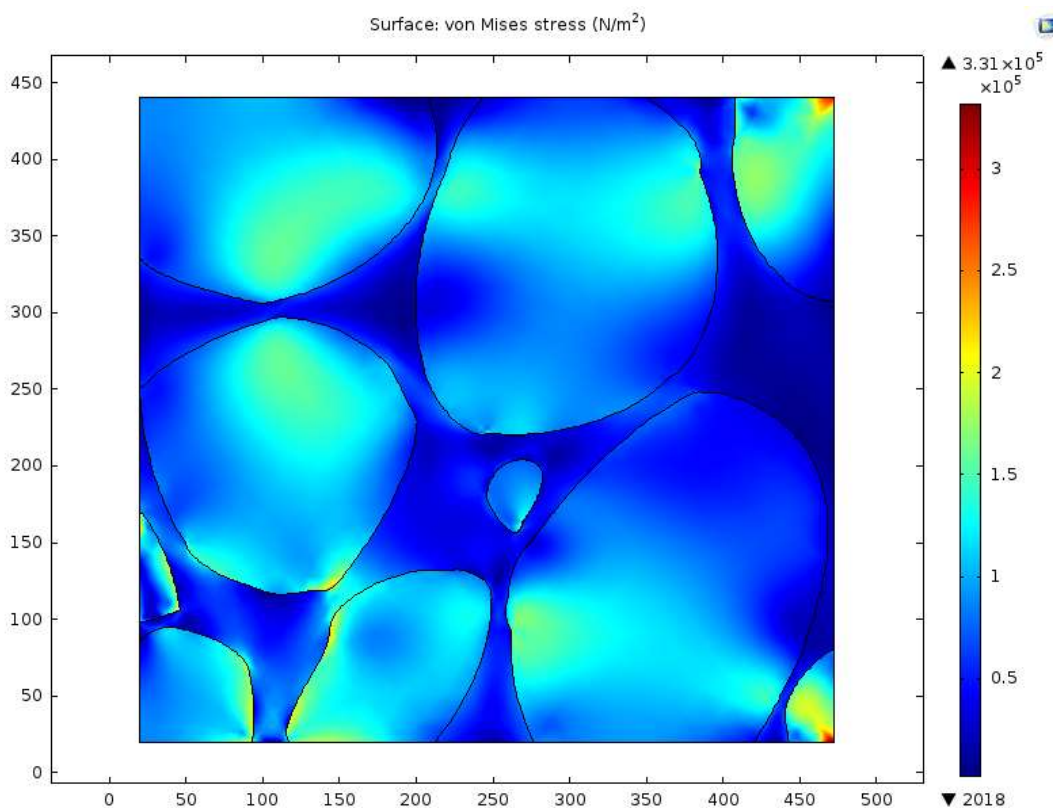


Figure 3.22. Final image with the stress values plotted which values are seen in the legend on the right hand side. The scale is in pascal.

Clearly the value of the stress varies across the sample, but is maximum within the ZnS particles, demonstrating good stress transfer between the PDMS and the particles. Not only is the high volume fraction of the particles clearly observed, but also it can be seen that the stresses depend on the shape of the particles, and the distance between each other. It is possible to quantify the stress in function of the distance between the particles. It is possible to see that at a distance of $0.25\mu\text{m}$ the stress as an average increase of 2.3 times and at a distance higher, for example around $0.75\mu\text{m}$, the increasing on the stresses is around 1.7 times. Moreover, an important consideration towards the shape is needed. As a matter of fact, geometry changes in a significant way the increasing of stresses. Indeed, where a less

rounded configuration is present, stresses reach higher level as it is possible to see from the figure 3.22 on the bottom left hand side where the intensification increase between 2 and 2.5 times even if they are at a distance between 0.75 and 1.25 μm distant.

3.5.1. Different stresses intensity with increasing number of particles.

A more detailed understanding can be further undertaken using idealised input geometries within COMSOL. Other simulations of different cases were consequently undertaken to see how the volume fraction of inorganic particles influence the behaviour of the stress intensity factor as shown in Figures 3.23-3.26. In these simulations different particle distributions, volume fractions and sizes were evaluated within the same area of the PDMS matrix of 20 X 20 μm . In these simulations the ideal case of complete bonding between the PDMS and ZnS is included.

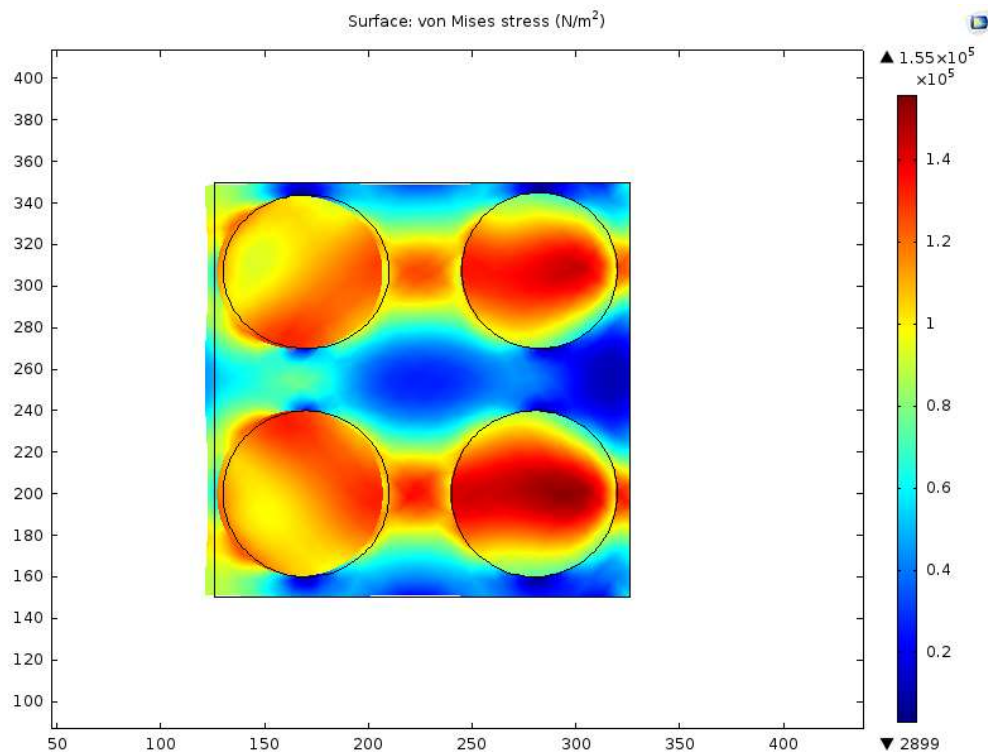


Figure 3.23. Ideal case distribution of four particles in the PDMS matrix

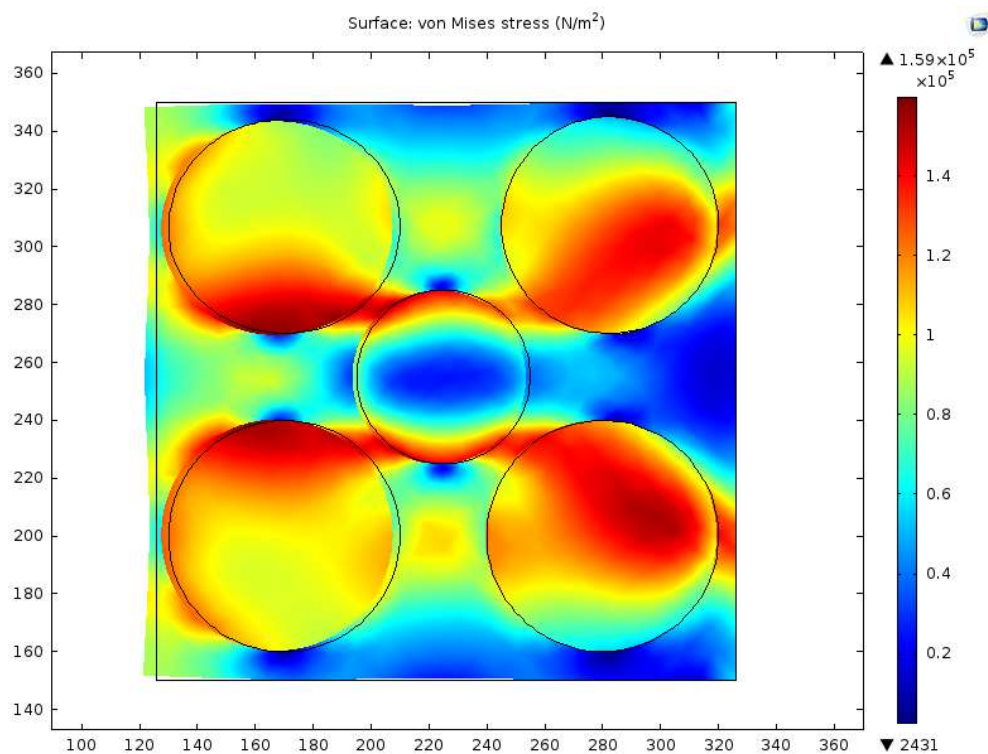


Figure 3.24. Five particles ideal case

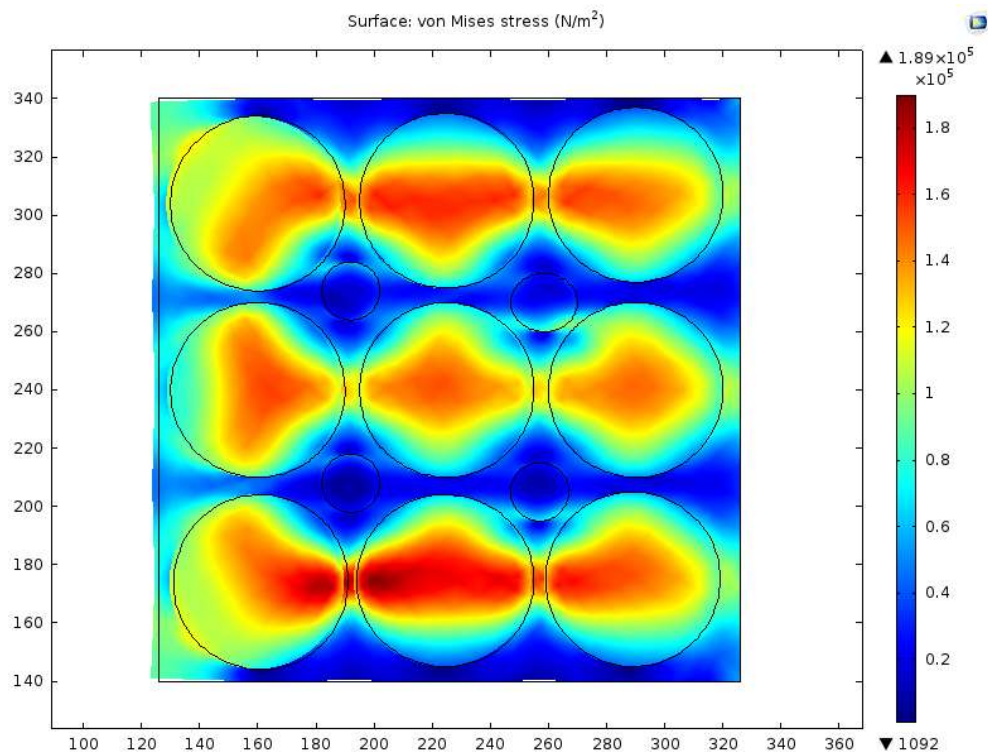


Figure 3.25. More volume fraction of ZnS dispersed in the PDMS matrix

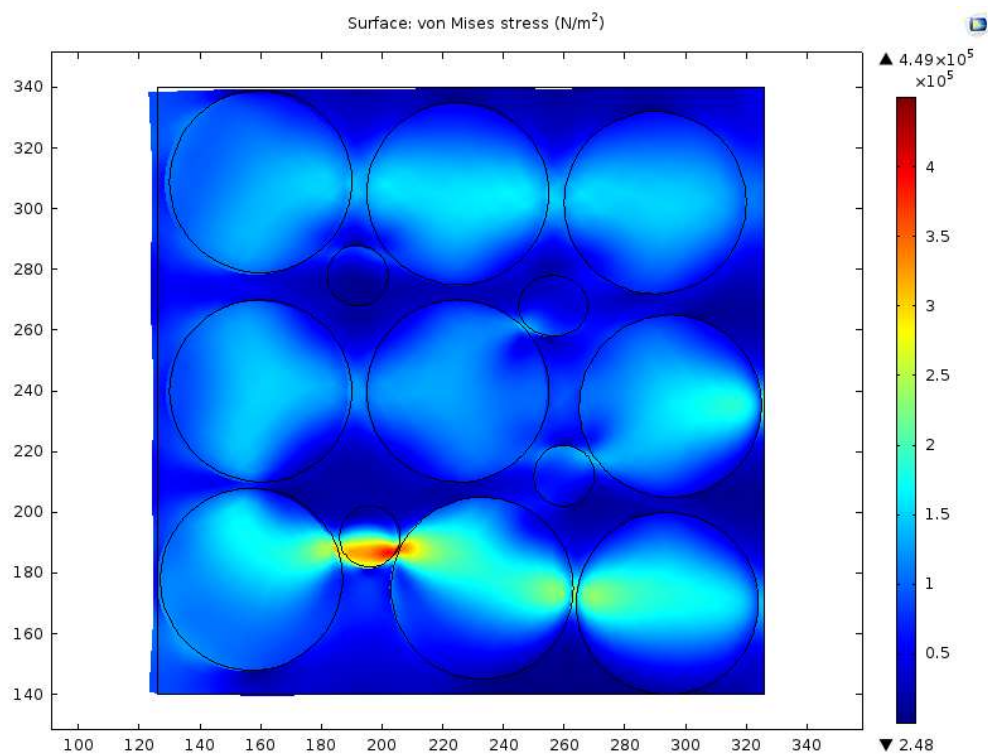


Figure 3.26. Random distribution with a tangent contact

In Figure 3.23 containing 4 large (8.5 microns diameter) particles with centers 12.8 microns apart, stress transfer is observed from the matrix to the particles. At an input strain of 0.1, maximum von Mises stress observed in the ZnS particles of 1.55×10^5 Pa. The low stress within the particles is very similar to the simulation of a single particle in the matrix calculated with Abaqus (see Section 3.2.1). Diminishing the size of particles and increasing their density higher stresses are seen as in the figure 3.24 and 3.25.

In the first situation, the volume fraction is increased, the four particles at the edges have a diameter of 8 microns while the one in the middle is 5.5 μm . A little increase respect to the previous case is present, but the difference is not high.

In picture 3.25 the situation is much different, there are nine particles of 6 μm of diameters and four particles of 1.8 microns. So, a situation of higher volume fraction of particles is represented. The intensification of stresses increases respect to the two previous cases, with a maximum value of almost 0.2 MPa.

Finally, in the picture 3.26 there is the situation of two particles in contact between each other and it is possible to clearly see a stress intensification and that the value obtained is around 0.5 MPa as the one obtained in the Abaqus simulation described in the Section 3.2.2.

3.6. Conclusions

With the finite element analysis with Abaqus and COMSOL it was possible to understand how the different density of inorganic particles in the PDMS influences the stresses experienced by the ZnS particles and also that the maximum stress intensification is reached when particles are touching each other

It is possible to see that the results obtained changed a lot in the different simulations and some important conclusions can be seen in the situation described in picture 3.1, so for an ideal particle with a round shape and no interaction with the surrounding inclusions, a maximum stress of 0.1 MPa is obtained

In the figures 3.23, 3.24, 3.25 it is possible to see how the volume fraction influence the stresses: the more the particles, the more the increasing of the stress. In the figure 3.22 it is possible to understand how the shapes influence as well the final result and so it is something to consider while making the modellization, values are almost 2 times higher with irregular shapes than the one in figure 3.25.

Finally, the condition that produce an increase of 5 times the stress is when two particles are in contact as represented in figure 3.9 and in figure 3.26 with a higher volume fraction of particles. This brings an increasing of stress up to five times.

In order to observe EML in ZnS:PDMS composites a threshold stress value must be exceeded in the ZnS. At stress values below this threshold value no ML is expected to be observed. Using the FEA simulations it is possible to obtain different stress values for various situations that might represent the real experimental conditions present in the PDMS:ZnS composites subjected to stress-strain behaviour experienced in the mechanical shaker.

As it was not possible to test the GG series phosphors in this thesis, data which matches the current settings has been evaluated and values of ML intensity versus the average stress have been extracted as shown in Figure 3.27 [1].

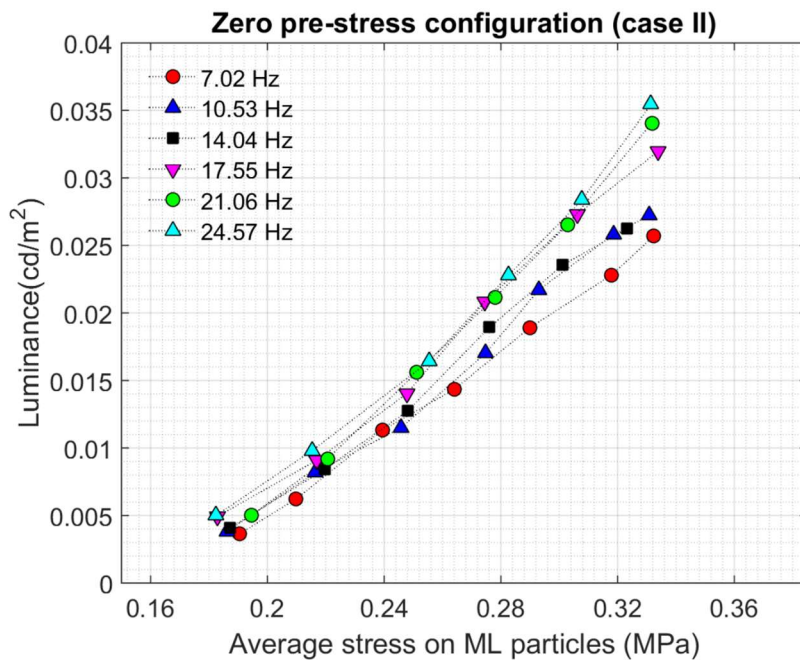


Figure 3.6.1. Experimental analysis made in the reference [1] where performed and stress vs intensity of the ML was plotted.

These data show (Figure 3.27) that there is linear relationship between the applied stress and the ML intensity. These data can be compared with the stress values obtained from the Abaqus and COMSOL simulations. In the single particle geometry calculations, a value of 0.1 MPa was observed when there was strong bonding between matrix and the ZnS, and based on the results of Figure 3.27 a ML intensity close to zero is expected. In the ideal case of two particles in contact, the stress is much higher with a value around 0.5 MPa. Comparing to Figure 3.27, it would be expected to observe significant luminescence intensity ie $> 0.34 \text{ cd/m}^2$.

These consideration let understand why there is the need of having a 7:3 ratio ZnS : PDMS: a high fraction of volume and in some case the contact between particles is needed to have a high value of emission due to mechanoluminescence.

The condition obtained with the homemade particles of a ratio 1:2 is not enough to recreate this situation and it might be a reason why EML phenomenon is not present in the samples (as we will see also in the next chapter).

References

- [1] Krishnan, S. (2015). Mechanoluminescent and Phosphorescent Paint Systems for Automotive and Naval Applications.
- [2] Soon, S., & Jeong, M. (2014). As featured in Energy & Environmental Science. *Energy & Environmental Science*, 7, 3338–3346.
- [3] Jha, P., & Chandra, B. P. (2013). Impulsive excitation of mechanoluminescence in SrAl₂O₄: Eu , Dy phosphors prepared by solid state reaction technique in reduction atmosphere. *Journal of Luminescence*, 143, 280–287.
- [4] Fincan, M. (2015). Assessing Viscoelastic Properties of Polydimethylsiloxane (PDMS) Using Loading and Unloading of the Macroscopic Compression Test.
- [5] Crystallography and Crystal Defects 2nd edition, Anthony A. Kelly, Kevin M. Knowles. Chapter 6, Stress, piezoelectricity and elasticity
- [6] J. Chu, T. Dietl, W.D. Dobrowolski, M. Rusu, T. Story and D. Strauch *New Data and Updates for several Semiconductors with Chalcopyrite Structure, for several II-VI Compounds and diluted magnetic IV-VI compounds*. Editor: U. Rössler. Semiconductors Subvolume F
- [7] Fontenot, R. S., Allison, S. W., Lynch, K. J., Hollerman, W. A., & Sabri, F. (2016). Mechanical, spectral, and luminescence properties of ZnS:Mn doped PDMS. *Journal of Luminescence*, 170, 194–199.
- [8] Jeong, S. M., Song, S., & Kim, H. (2016). Simultaneous dual-channel blue/green emission from electro-mechanically powered elastomeric zinc sulphide composite. *Nano Energy*, 21, 154–161.
- [9] Moon Jeong, S., Song, S., Lee, S. K., & Choi, B. (2013). Mechanically driven light-generator with high durability. *Applied Physics Letters*, 102(5). Peng, W. Q., Cong, G. W., Qu, S. C., & Wang, Z. G. (2006). Synthesis and photoluminescence of ZnS:Cu nanoparticles. *Optical Materials*, 29(2-3), 313–317.
- [10] Highly stretchable and self-deformable alternating current electroluminescent devices. *Advanced Materials*, 27(18), 2876–2882.
- [11] Wang, W., Huang, F., Xia, Y., & Wang, A. (2008). Photophysical and photoluminescence properties of co-activated ZnS:Cu,Mn phosphors. *Journal of Luminescence*, 128(4), 610–614.

[12] Evaluation and benchmark for biological image segmentation Elisa Drelie Gelasca, Jiyun Byun, Boguslaw Obara, B. S. Manjunath University of California, Santa Barbara 93106-9560 (n.d.), 1–4.

[13] Sciences, D., Africa, S., & Africa, S. (2011). Fingerprint segmentation: an investigation of various, 7(9), 5313–5326.

4. New theory for mechanoluminescence in doped ZnS

The aim of this last chapter is to propose a new theory of the mechanism behind mechanoluminescence and to try to produce working EML ZnS doped particles.

There are a lot of mechanoluminescent phosphors that are commercially available, that are both organic and inorganic and with different types of structure and containing different kinds of dopants [1]

Particular attention in this thesis is given to the ML phosphors that have been used in most papers where devices with PDMS have been fabricated [2-6]. These are ZnS doped materials of the GG series, sold by GTP Corp, and have been used because of their high emission intensity and low stress threshold to see the phenomenon. These are the most promising phosphors since they are the only inorganic ML materials that when embedded in PDMS show the phenomena with a very low stress. In Chapters 1 and 2, the ML theory proposed by Chandra regarding mechanoluminescence was discussed. It is not very clear according to its theory how the electrons are able to jump from their energy level to the conduction band and what is the minimum stress values at which the ML is seen. There is also no single mechanism for all ML systems with different mechanisms for each type of phosphor. This chapter focussing solely only the ZnS doped ML materials.

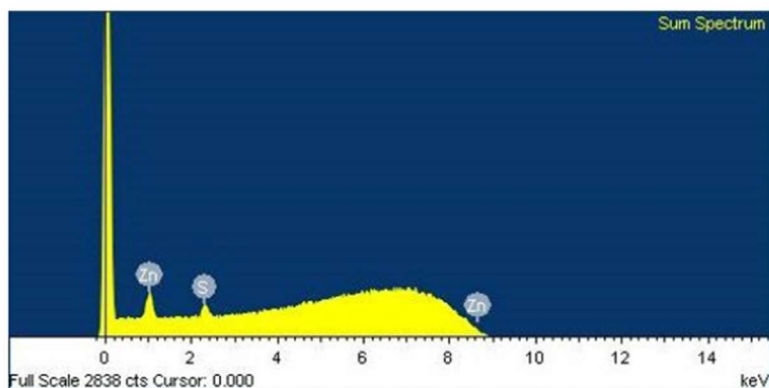
4.1. Evidence in literature

Looking at the different ZnS phosphors available on the market it is possible to see that there are different kinds of doped ZnS. Those from GTP Corp., known commercially as GG13 and

GG25 are widely used in the production of ML devices because a relative small amount of stress is sufficient to induce the phenomenon. The phosphor known as GL 25 from Phosphor Technology Ltd UK, is not used for ML applications because the stress needed to induce mechanoluminescence is very high, and exceeds and the stresses that can be achieved in the ZnS when embedded in PDMS. Therefore, it is at first necessary to study what the difference between these two kinds of material are, even if they appear to be nominally the same material.

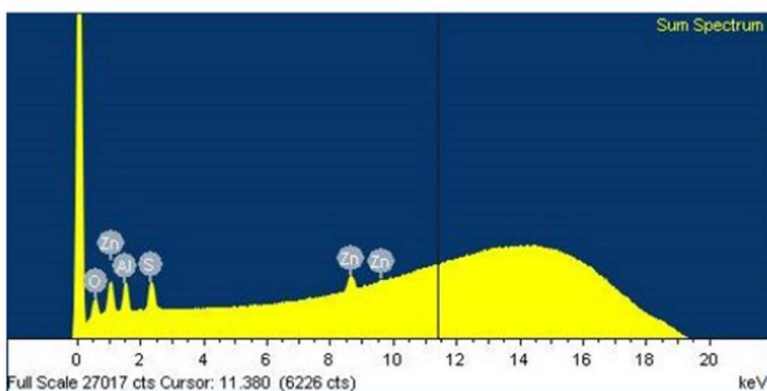
The GG and GL phosphors have been studied by the EDS spectra (Energy Dispersive X-ray Spectrometry) [7]. EDS is a technique that analyses x-rays emitted from a specimen when an electron or proton beam collide with it to determine the chemical make up of the sample being analysed. [8]

The results of this work are reproduced in Figures 4.1-4.3. These data show that there is clear the distinction in the composition between the GL25, then the GG13 and the GG25 phosphors.



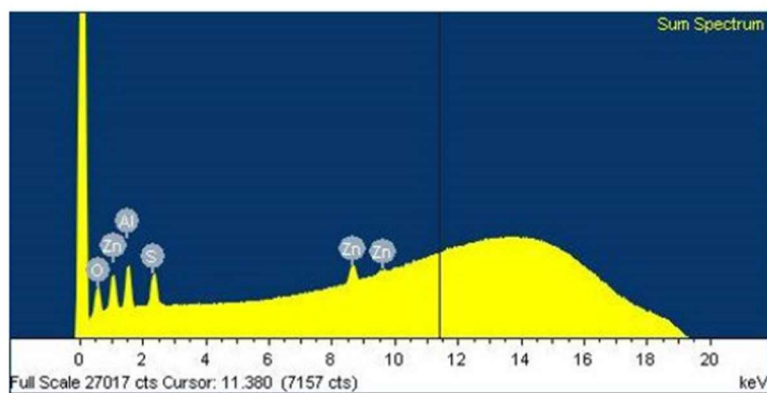
Element	Wt %	At %
Zn	65.52	48.24
S	34.48	51.76
Total	100	100

Figure 4.1. EDS spectra of GL 25 phosphors (reproduced from Reference [7])



Element	Wt %	At %
Zn	44.13	20.33
S	13.51	12.69
Al	16.65	18.58
O	25.71	48.39
Total	100	99.99

Figure 4.2. EDS spectra of GG13 phosphor (reproduced from Reference [7])



Element	Wt %	At %
Zn	40.54	17.80
S	12.27	10.98
Al	18.43	19.61
O	28.77	51.61
Total	100	100

Figure 4.3. EDS spectra of GG25 phosphor (reproduced from Reference [7])

These data show that there are differences in percentage of the Zn and S atoms between the GG and GL series. In addition, whilst in the GL series only Zn and S are detected, in the GG series significant percentages of both Al and O are present. Interestingly the dopants atoms known to be present in these phosphors are not observed in the EDS analysis, presumably because they are at too low percentage.

Analysis of the structure of the GTP Corp phosphors using TEM imaging [9], clearly shows that the ZnS particles are coated by an Al layer that is a ~400 nm thick as shown Figure 4.4.

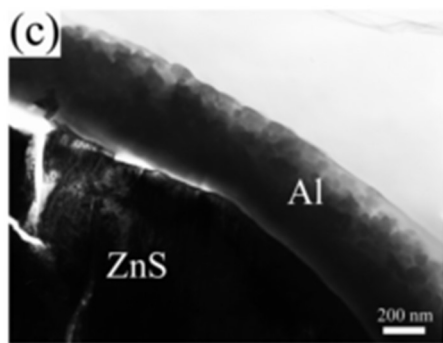


Figure 4.4. ZnS powders from a TEM analysis. The ZnS particle is covered with an Al layer.

These authors also used an EDS technique to analyse the composition, and found that the percentage ratio of Cu : Zn : S :Al was 0.063:53.1:30.3:16.45 [9]. This Al layer is actually the key material to obtain bright luminescence intensity phosphors that have a low stress threshold for ML emission. Since Al is not present for example in the GL series, these conditions are not observed in these materials.

From these reports in the literature, it is possible to conclude that for these ML materials, a coating is a necessary requirement for high luminance and low threshold stress ML materials. Indeed, the supposition is that there must be a physical link between the semiconductor and the metal. It is also seen from the EDS analysis a large quantity of oxygen is present, which is most likely in the form of alumina compounds, i.e. making the Al-coating an insulator material. Though, the only way in which these particles can work is with a physical link between semiconductor and metals as it will be proven later in this chapter. This implies that the alumina is present in only a small percentage with respect to the metallic aluminium. The semiconductor therefore provides the recombination centres within the energy gap that permits the emission of light, whilst the metal provides the electrons at reduced stress and in a quantity such that a higher luminescence intensity can be seen. This can occur with only a small electric field due to the piezoelectric effect.

The physical junction between semiconductor and metal is a so-called Shottky diode whose behaviour is well understood and is explained in the section below.

4.2. Shottky Diode

The Shottky diode is named after the German physician Walter Shottky and it is a low tension diode with a high switching action. Usually the typical forward voltage is around 150-450 mV and this is the reason for its high switching speed and gives a more efficient system. A band diagram helps explain the phenomenon as shown in Figure 4.5. [10]

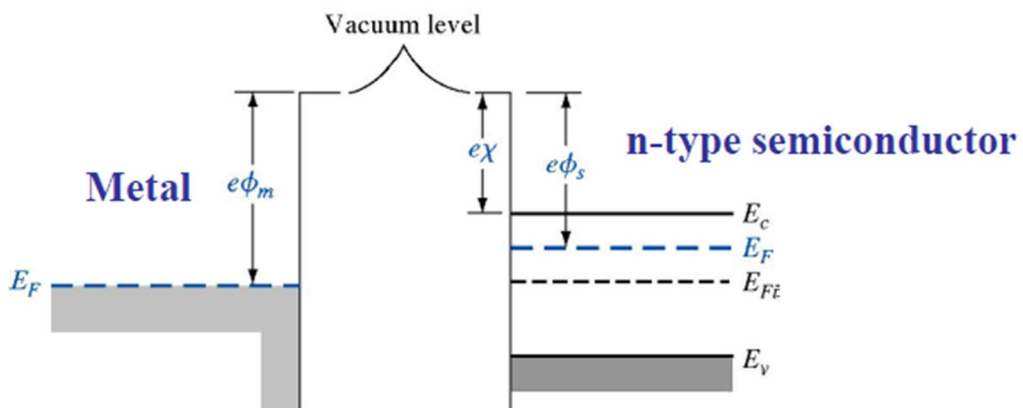


Figure 4.5. Metal and Semiconductor diagrams and variables. On the left hand side, the metal Fermi energy and its work function while on the right hand side the n-type semiconductor band structure is represented [10]

The work function, ϕ , is the energy needed to move an electron from the Fermi energy level into vacuum level, and the electron affinity, χ , is the energy needed to move an electron from the semiconductor conduction band into the vacuum band.

All physical constants such as ϕ and χ are known and have been tabulated for many different materials including Al and ZnS.

As shown in Figure 4.5, the metal and the semiconductor are in a condition where they are separated, meaning that there is no physical junction between them. The energy level diagram only shows the difference in the fermi energy levels and in the band structure.

When a physical junction is present between the two materials, the situation changes to that shown in Figure 4.6, where it is possible to see a distortion of the bands. [10]

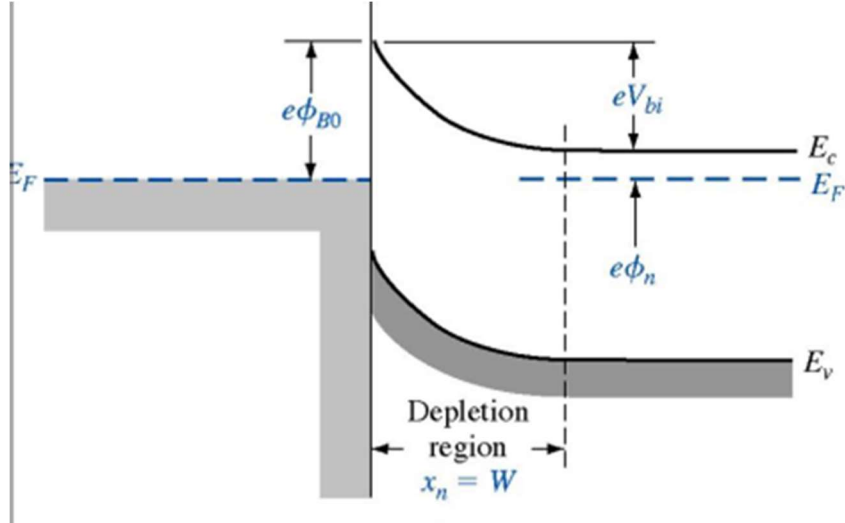


Figure 4.6. When metal and semiconductor are in contact, there is a change in the Fermi level and the bending of the energy levels. [10]

When there is separation between the two materials (Figure 4.5), an n-type semiconductor is present, the fermi energy of which is higher than that for the metal and so the electrons will flow from the semiconductor to the metal. When the two materials are coupled (Figure 4.6) a change in the Fermi level is observed that reaches the same level after the coupling and the bending of the energy levels. Moreover, a space charge region in between is created called the depletion region. This is an insulating region where the charge carriers are not present, but diffuse away. The only elements that are present are ionized donor or acceptor impurities, so together with negative and positive charges an electric field is generated.

Given this, it is now possible to define the Shottky Barrier as the potential barrier which electrons in the metal experience in trying to move into the semiconductor. The magnitude of the barrier is given by $\phi_{B0} = \phi_m - \chi$. Moreover, the increase in potential barrier height is the potential barrier which electrons in the semiconductor experience in trying to move to the metal and given by $V_{bi} = \phi_{B0} - \phi_n$.

When a bias is applied to the system, two conditions might occur depending on the sign of the bias, i.e. a reverse or a forward bias can be applied. Hence, if a positive voltage is applied to the semiconductor, the barrier between the semiconductor and the metal increases while the Shottky barrier remains unchanged. The relation $V_f = V_{bi} + V_R$ is found where V_{bi} is the built-in potential, V_R is the applied voltage and V_f the resulting value. In this situation, the electrons will see a higher barrier that needs to be overcome to be able to flow in the metal. [10]

In the case of a negative bias being applied, then the metal barrier decreases and the resulting voltage is given by $V_f = V_{bi} - V_R$, hence, the flow of the electrons will be easier than under a positive bias.

As discussed above, in the depletion region there are positive and negative charges that cause an electric field. This electric field helps the electrons to move from the semiconductor to the metal providing a current density. There will simultaneously be a current density in the opposite direction, but its magnitude is much less than the one in the direction of the electric field. Moreover, the combination of these fields is to modify the band diagram as shown in Figure 4.7 forming a difference of $\Delta\phi$ in the Shottky barrier values [10].

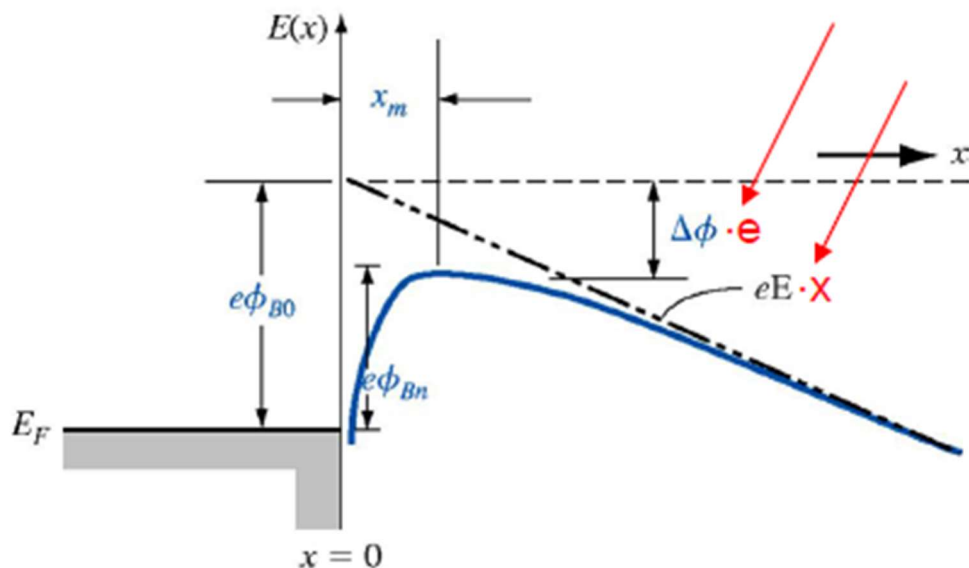


Figure 4.7. Barrier banding due to the electric field generated in the depletion region, Reproduced from reference [10]

The situation shown in Figure 4.7 is one possible condition that can happen when contact between a semiconductor and a metal is present. Three other possible situations that could exist are shown in Figure 4.8, showing energy levels for n-type and p-type ohmic and rectifying junctions.

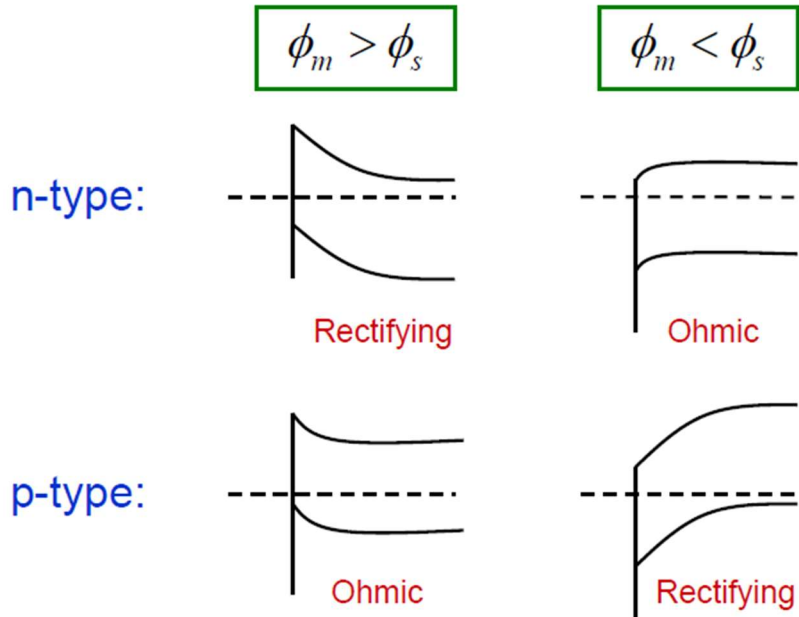


Figure 4.8. Possible situation of the semiconductor to metal connection [10]

The difference between the ohmic and the rectifying systems lies in the fact that the ohmic one permits the flow of currents in both directions, while the rectifying one does not. [10]

4.3. Doped ZnS covered with Al

When ZnS is coated with Al a slightly different situation exists as shown in Figure 4.9. Given knowledge of the work function and constants for ZnS and Al, it is possible to construct a barrier diagram as shown in Figure 4.9 [9].

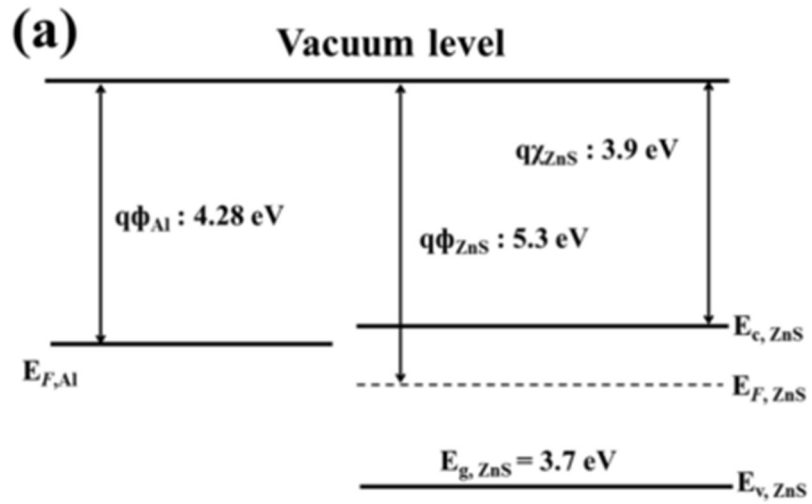


Figure 4.9. Band diagram of ZnS doped and Al [9]

Due to the fact that the fermi energy of Al is higher than the ZnS semiconductor, then the electrons will flow from the metal to the semiconductor. When these materials are in contact, there is a bending in the energy levels giving the situation shown in Figure 4.10.

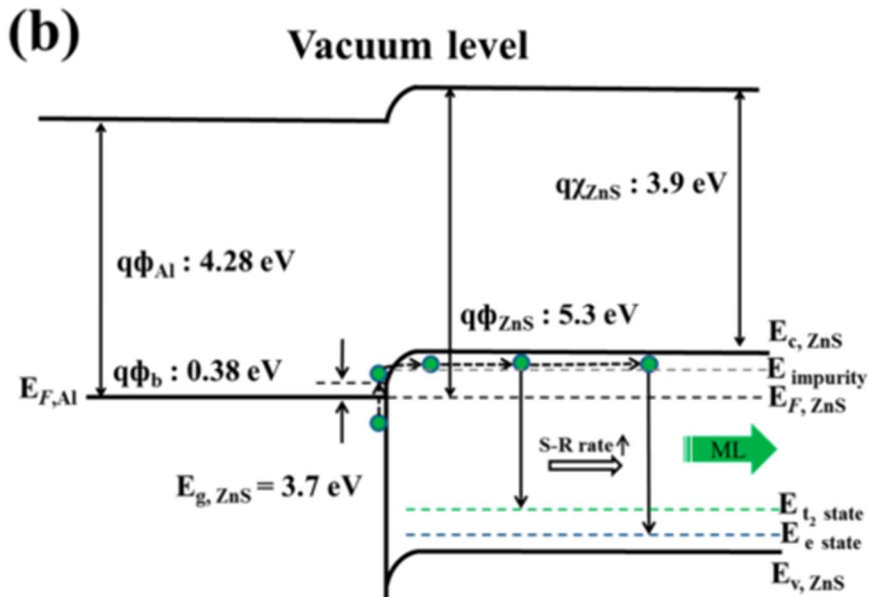


Figure 4.10. ZnS doped and Al after the physical contact [9]

For a *p*-type material with a Fermi energy of the semiconductor that is lower than that of the metal, a rectifying contact forms so that the flow of current is permitted in only one direction.

Further consideration can be made regarding the two energy states t_2 and e . These are common names given to the orbitals in polyatomic molecules according to their symmetry. The t_2 state denotes a doubly degenerate orbital, i.e. two orbitals with the same energy, whilst the e state indicates a triply degenerate orbital, i.e. where three orbitals have the same energy. [11]

This implies that two recombination states are present in the system. Hence, when a low CPM (Cycles per minute) rate occurs, then the recombination between electrons and holes happens at the t_2 state in preference to the e state. At higher CPM rates, then more electrons are produced, so that the t_2 state gets filled very quickly and hence, the electrons also recombine with the holes of the e state [9]. This effect explains the change in of colour of ML that has been observed at different CPM rates [12].

From the FEA simulation results some strength values between 0.1 and 0.5 MPa are obtained and it is possible to see if the electric field generated from the piezoelectric effect is enough to bring a movement of electrons from the metal to the semiconductor following the Shottky theory.

The piezoelectric effect is described by a constitutive equation that links the charge density, the stresses and the electric field with the properties of the material [13]:

$$\mathbf{T} = \mathbf{d} \cdot \boldsymbol{\sigma} + \mathbf{e} \cdot \mathbf{E}$$

Equation 4.1. Constitutive equation of the piezoelectric effect linking charge density, electric field and the stresses with the material properties.

Where \mathbf{T} is the charge density, $\boldsymbol{\sigma}$ is the stress, \mathbf{e} the permittivity of the material, \mathbf{d} is the compliance and \mathbf{E} is the electric field.

When the circuit is not connected to any circuit, then the T value is zero so the equation permits with our parameters to find the electric field generated with a certain stress.

$$E = - \frac{d \cdot \sigma}{e}.$$

Equation 4.2. Electric field induced with the piezoelectric effect.

Values of the stress are taken from the Comsol modellization in the non-ideal case seen in picture 3.22.

Since for ZnS, $d = 3.3 \times 10^{-12}$ C/N and knowing that $e = 8.7 \times 10^{-12}$ CV/m, using Equation 4.2 gives a value of $E = -1.2 \times 10^4$ V/m. This is the electric field generated inside the material and since the particles have a radius of 20 μm then the voltage due to the electric field given by:

$$E \cdot m = V$$

Equation 4.2. Relation electric field to voltage.

where m is the dimension of the geometry over which the field is applied, in this case the ZnS particles. Substitution of the field and particle size into Equation 4.3 gives a voltage of 0.24 V.

No precise value for the threshold voltage that permits flow of electrons in these systems has been reported, but estimates give this value in the range of millivolts. If this is true, then the estimate for the voltage observed in the COMSOL simulation (240 mV) would be more than sufficient for flow of electrons from the metal to the semiconductor to occur. Moreover, the negative bias in the semiconductor means a decreased barrier height, making it even easier for the electrons to flow from the metal to the semiconductor. As a matter of fact, the situation described in Figure 4.10 would be additionally altered due to bending in the energy levels as shown in Figure 4.11 [10].

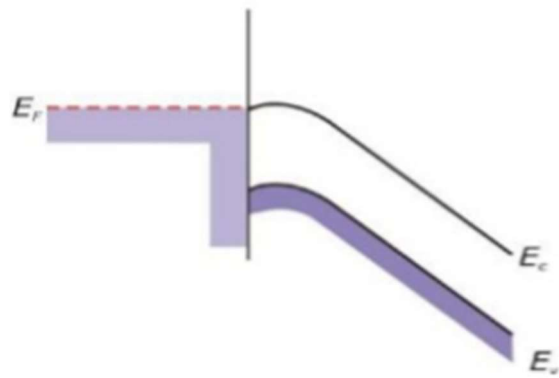


Figure 4.11. Reverse bias condition of ohmic contact with p-type material. Reproduced from reference 10.

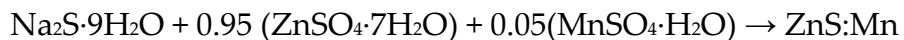
4.4. Experimentation to prove the theory.

To support the validity of the theory synthesis of EML powders with precisely known chemical compositions is necessary> A range of ZnS materials both with and without dopants were synthesized in house by Laura English. The procedure for synthesising the doped ZnS powders followed the methods in the literature [15]. Neither the pure ZnS or the doped ZnS powders showed any mechanoluminescence that could be detected either by the Flame UV-vis spectrometer or by eye.

The synthesis utilized by English [15] is summarized below:

First 10g of sodium sulphide nonahydrate ($\text{Na}_2\text{S}\cdot 9\text{H}_2\text{O}$) were dissolved in 50 mL of distilled water, and 9.5g of zinc sulphate heptahydrate ($\text{ZnSO}_4\cdot 7\text{H}_2\text{O}$) and 0.5g of manganese sulphate monohydrate ($\text{MnSO}_4\cdot \text{H}_2\text{O}$) in 50 mL of water. Both solutions were stirred for 1 hour before pouring the sodium sulphide solution into the zinc and manganese sulphate solution.

The reaction that occurs is:



This was then left to stir for 4 hours, before adding 50 mL of methanol and then left to settle overnight.

Then the top layer was discarded and the remaining solution divided between test tubes and centrifuged at 1000rpm for 20 minutes. The liquid was discarded and the solid washed with methanol before centrifuging again. This was repeated four times, and then another five times using distilled water instead of methanol. The solid was then collected and left to dry at 100°C overnight.

To coat the ZnS particles with Al, aluminium added to the ZnS equal to 16-18% by weight. These were ground together using a mortar and pestle, then cold pressed into a pellet and vacuum sealed into a quartz tube. This solid is then placed in the furnace for 2 hours at 700°C (heating rate = 20°C/min, cooling rate = 20°C/min) in a vacuum sealed quartz tube. On completion of the annealing, the quartz tube is broken open to form the grey powder shown in Figure 4.12.

All the reagents were purchased by Sigma Aldrich, except the aluminium powder which is from Fischer Scientific.

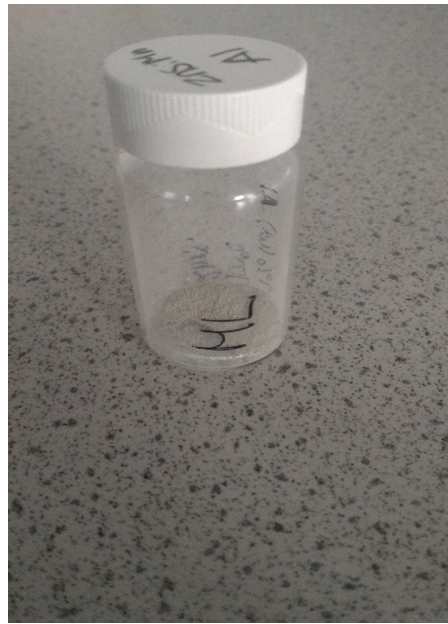


Figure 4.12. ZnS:Mn via liquid reaction coated with Al

An alternative route, was tried using solid state reaction was taken to make the same powders. In this method, 0.1690g of sulphur powder, 0.0276g of manganese powder and 0.3309g of zinc powder were ground together in a mortar and pestle. This was then cold pressed into a pellet and vacuum sealed in a quartz tube. The tube was then placed in the furnace for 6 hours at 650°C (heating at 25 degrees/minute and cooling at 10 degrees/minute).

Some of the resulting powder (0.2538g) was ground together with 0.0474g of aluminium powder and cold pressed into a pellet and vacuum sealed in a quartz tube. This sample was then placed in the furnace for 2 hours at 700°C (heating at 20 degrees/minute and cooling at 20 degrees/minute) i.e. 40 °C above the melt point of Al.

The sulphur powder and the zinc powder were both purchased from Sigma Aldrich and the manganese powder from Alfa Aesar. The resulting grey solid powder is shown in Figure 4.13 and has a very similar in colour to the undoped ZnS/Al sample.



Figure 4.13. ZnS:Mn with Al via Solid state reaction

To check for mechanoluminescence, a glass rod was used to apply a localized compressive force to the powders. Orange mechanoluminescence emission was clearly seen for both from the solid state processed and the solution synthesized doped ZnS after Al coating as shown in Figure 4.14.



Figure 4.14. Orange light emission from the EML ZnS/Al powders produced by solid state reaction on the left hand side and solution processes.

These ML active powders were also embedded in PDMS matrices. It was not possible to form composites with the desired 7:3 weight ratio of ZnS particles to PDMS (see discussion above) so a 1:2 ratio was used instead. Although the particles demonstrated mechanoluminescence in their native state, when incorporated with PDMS these composites did not produce any visible luminescence either by eye or using the UV-vis spectrometer also of the particles.

Conclusion

A theory based on Shotky diode principles has been proposed. This theory indicates that Al as a coating is a necessity for ML activity in doped ZnS materials. Al coated doped ZnS were evaluated and compared to both undoped ZnS and also uncoated doped ZnS. Only when

the Al coating is present was it possible to see emission of light from these materials. It means that the theory is correct and as predicted the wavelength emitted is in the right range being ZnS:Mn doped particles.

For mechanoluminescence in these materials, the stress threshold to have light emission is clearly decreased, permitting emission phenomenon in the particles. However, mechanoluminescence was not observed in the ZnS:PDMS composite samples. Further analysis and studies will be needed to understand why luminescence was not observed in the composites. One obvious explanation is that with a 1:2 loading ratio (well below the desired 7:3 used successfully by other groups) the particles are not close enough to exceed the minimum stress required to cause light emission after mechanical excitation. Moreover, another cause is that, since analysis of the structure were impossible to perform due to lacking of time, it might be that the percentage of fully covered ZnS doped powders with Al is low and so limited numbers of particles show ML. Clearly more analysis is needed to show what has occurred during the reaction to better understand it and improve the production process.

References

- [1] Zhiyong Ma, Zhijian Wang, Dr. Mingjun Teng, Dr. Zejun Xu, Prof. Xinru Jia. Mechanically Induced Multicolor Change of Luminescent Materials *ChemPhysChem* 9/2015
- [2] Soon, S., & Jeong, M. (2014). Bright, wind-driven white mechanoluminescence from zinc sulphide microparticles embedded in a polydimethylsiloxane elastomer. *Energy & Environmental Science*, 7, 3338–3346.
- [3] Fontenot, R. S., Allison, S. W., Lynch, K. J., Hollerman, W. A., & Sabri, F. (2016). Mechanical, spectral, and luminescence properties of ZnS:Mn doped PDMS. *Journal of Luminescence*, 170, 194–199.
- [4] Jeong, S. M., Song, S., & Kim, H. (2016). Simultaneous dual-channel blue/green emission from electro-mechanically powered elastomeric zinc sulphide composite. *Nano Energy*, 21, 154–161.
- [5] Moon Jeong, S., Song, S., Lee, S. K., & Choi, B. (2013). Mechanically driven light-generator with high durability. *Applied Physics Letters*, 102(5). Peng, W. Q., Cong, G. W., Qu, S. C., & Wang, Z. G. (2006). Synthesis and photoluminescence of ZnS:Cu nanoparticles. *Optical Materials*, 29(2-3), 313–317.
- [6] Wang, Jiangxin Yan, Chaoyi Chee, Kenji Jianzhi Lee, Pooi See. Highly stretchable and self-deformable alternating current electroluminescent devices. *Advanced Materials*, 27(18), 2876–2882.
- [7] Krishnan, S. (2015). Mechanoluminescent and Phosphorescent Paint Systems for Automotive and Naval Applications.
- [8] Notes and slides from Mirella Del Zoppo. Associate professor, Dipartimento di Chimica, Materiali ed Ingegneria Chimica “G.Natta”. Politecnico di Milano.
- [9] Shin, S. W., Oh, J. P., Hong, C. W., Kim, E. M., Woo, J. J., Heo, G.-S., & Kim, J. H. (2016). Origin of Mechanoluminescence from Cu-Doped ZnS Particles Embedded in an Elastomer Film and Its Application in Flexible Electro-mechanoluminescent Lighting Devices. *ACS Applied Materials & Interfaces*, 8(2), 1098–1103.
- [10] Notes and slides from Sanjay Ram teacher at Aarhus university, Physics department
- [11] Atkins, Overton, Rourke, Weller, Armstrong. Inorganic Chemistry Shiver & Atkins fifth edition. Published in 2010 in Great Britain by Oxford University Press.
- [12] Jeong, Soon Moon Song, Seongkyu Kim, Hyunmin. Simultaneous dual-channel blue/green emission from electro-mechanically powered elastomeric zinc sulphide composite. *Nano Energy* Volume 21, pages 154-161. 2016

[13] Lecture and note of Cinzia Cristiani. Associate professor. Dipartimenti di Chimica, Materiali ed Ingegneria Chimica "G.Natta" Politecnico di Milano

[14] S.Ummartyotin et. Al. Synthesis and Luminescence properties of ZnS and Metal (Cu,Mn) doped ZnS ceramic powder. Solid State Sciences Volume 14, Issue 3, March 2012, Pages 299–304

[15] L. English, A Study of the Synthesis and Properties of zinc sulphide, Private communication, August 2016

5. General conclusions and further studies

ZnS doped particles are a promising mechanoluminescent materials, because they show the phenomena even at very low stresses and deformation. Their study is therefore important to create high efficiency devices that show the phenomenon. The dopants and coatings required for active materials are also reasonably cheap and widely available.

Alternative ML materials that have been studied, i.e. SrAl₂O₄:(Eu,Dy) and MoAl₂O₄:(Eu,Dy) display similar luminescent characteristics, and can be classified into either permanent or instantaneous mechanoluminescence materials. The stress needed to produce EML in these materials is however higher than that needed for the ZnS doped systems. Similar wavelength emissions for all the ML materials studied was observed. It is important to note that the emission colour depends on the dopant only, and not on the crystalline structure. Similar colours result as a consequence of similar energy levels gaps within the systems.

An initial wider aim of the project was to study ZnS mechanoluminescent particles embedded in PDMS to make elastic low stress ML devices. To understand and optimize such systems necessitated the use of FEA modelling, which was used to evaluate the stress distribution inside the materials and determine the threshold stress to achieve the ML effect.

To perform the correct finite element analysis in PDMS:inorganic particles composites, Abaqus was initially used to simulate simple ideal geometries. These models clearly showed that to achieve stress levels in the particles that exceed those required for light emission, either direct contact or close proximity between the particles is necessary.

More accurate analysis was performed using COMSOL based simulations, based on an input model that derived from an experimental microscopy image from a real system. Software code was written (in Python) and together with Matlab the experimental image was meshed and imported into COMSOL in order to perform the finite element analysis. Based on these results further simulations using COMSOL was performed on more

idealised system to understand the effect of separation, dimension and volume fraction of particles in the polymeric matrix.

With the values obtained from the modelling together with additional evidence found in literature a working mechanism of mechanoluminescent particles was hypothesised. This hypothesis was to estimate the voltage created with the induced electric field from these piezoelectric materials. The resulting field (of order 240 mV) was shown to be of sufficient magnitude that if the ZnS doped particles are indeed coated with a metal such as aluminium, the required stress threshold to ultimately permit observation of mechanoluminescence would be surpassed. This situation is the equivalent of a Shottky diode, which works with very low voltage thresholds.

An experimental proof of the theory was performed on well-defined doped-ZnS particles that were synthesized and coated with Al. The experimental results confirmed the theory and demonstrated mechanoluminescence only in doped-ZnS when coated in Al.

Further studies are still needed to fully characterize the in-house synthesized ZnS doped and coated particles using among other techniques TEM and EDS analysis. It would also be important to study the percentage of coating of the powders and the size and regularity of the shapes of the particles in order to improve the production process.

Finally, the Abaqus and COMSOL models in this thesis, whilst providing the information required for this study are still approximate, and further studies to create appropriate 3D models and simulations from experimental samples as well as ideal geometries are needed to understand and better map and quantify the stress transfer between matrix and the inorganic particles. A much needed parameter is of course the strength of the bonding between the PDMS and the ZnS particles, in this thesis it was necessary to explore either no bonding or full bonding, i.e. idealistic situation of extremes that are unlikely to be true in real systems. Further studies to determine the adhesive strength of this interface are required in order to perform more realistic and accurate simulations.